

Analytical study of gravitational lensing in Kerr-Newman black-bounce spacetime

Saptaswa Ghosh¹, Arpan Bhattacharyya²

Indian Institute of Technology, Gandhinagar, Gujarat-382355, India

ABSTRACT

We investigate the equatorial deflection angle of light rays propagating in Kerr-Newman black-bounce spacetime. Furthermore, we analyze the light ray trajectories and derive a closed-form formula for deflection angle in terms of elliptic integrals. The deflection angle increases with the decrease of charge and regularisation parameter for a particular impact parameter. We also study the strong field limit of the deflection angle. Using this strong deflection angle formula and lens equation, we find the radius of the first Einstein ring and study its dependence on the charge and the regularisation parameter. We demonstrate that the charge has a robust effect on the size of the Einstein rings, but the effect of the regularization parameter on the ring size is negligible. We also investigate the non-equatorial lensing and the caustic structures for small polar inclination, and the same observations appear to hold. These results directly affect the observational appearance of the Kerr-Newman black-bounce.

¹saptaswaghosh@iitgn.ac.in

²abhattacharyya@iitgn.ac.in

Contents

1	Introduction	1
2	Null geodesics in the Kerr-Newman black-bounce spacetime	4
3	Computation of deflection angle: Analytical approach	9
4	Strong deflection analysis of equatorial lensing	14
5	Observational signatures in strong deflection limit	21
6	Strong deflection analysis of non-equatorial lensing	23
7	Analysis of the observables for the shadow	25
8	Discussions	29
A	Appendix 1: Details of the integrals used in Section (3)	31

1 Introduction

Black holes arising out as solutions to Einstein’s theory of General Relativity are an important testbed to probe into the intricate structures of spacetime. However, finding such objects was a great challenge until EHT gave us the first glimpse. Going on to the other way of getting data regarding such objects also gives us insight into which gravity theory observation of such objects provides essential data to ensure we are on the correct path. However, the recent developments in gravitational-wave astronomy ensure that such entities exist in nature. The shreds of evidence come from the set of detections of gravitational waves from binary black holes by LIGO, Virgo and KAGRA Collaboration [1–6]. Also, we have enough observational evidence that ensures the existence of supermassive black holes at the centre of our Milky Way galaxy. In recent times, “Event Horizon Telescope” (EHT) collaboration has given us the observational signatures of such kinds supermassive black holes [7–19]. Together with the data from LIGO-Virgo-KAGRA, these observations provide a unique opportunity to test various aspects of our theoretical predictions, particularly in the strong gravity regime [20–30].

The deflection of light in a gravitational field is one of the significant consequences of General Relativity, technically called gravitational lensing. One typically uses geometrical optics approximation to compute the deflection angle [31]. It can be shown that the deflection angle of light by some astrophysical objects depends on the distance between the object and the observer. Also, it depends on the parameters of underlying astrophysical objects. So, by calculating the deflection angle, one can estimate the parameters (spin, charge, mass), and by matching these with the observational data, one can validate a theory of gravity. It could provide observational constraints on theories beyond general relativity in some regimes [32–34]. The calculation of the exact deflection angle is complicated for an arbitrary metric. Hence, we must make assumptions by considering what kind of object we are looking for [31, 35–38].

The theory of gravitational lensing in the weak field limit was already developed in [39] long ago. It helps us estimate the parameters of less massive objects like stars and galaxies. However, the treatment fails when the objects are very compact and massive. Then we need to consider the strong field limit of deflection angle. In recent days, investigating the strong field limit of bending angle has become crucial since it could provide us with fundamental properties of supermassive objects like black holes. Based on the work [31] and [37] an analytical description of the deflection angle in the strong gravitational field has been proposed in [38], where the authors have shown the deflection angle logarithmically diverges when the turning point of the light rays gets close to the photon sphere. In [38], this analysis was presented for spherically symmetric black hole. Furthermore, this work was extended for rotating black hole in [40]. Treating black holes as lens, a lens equation has been derived in [31] and further corrected and generalized in [41]. Further analysis, including investigation of Einstein rings [42], of the lens equation, and strong gravitational lensing based on the work [40], has been made for various black hole spacetimes and compact objects [43–80]. Another consequence of the strong deflection analysis is the investigation of black hole shadow, a two-dimensional dark zone in the celestial sphere caused by the strong lensing of the black hole, which is a dark silhouette of the BH against a bright background. Although we will use this particular notion of shadow in this paper following [7], there are other formulations to quantify the visual appearance of a black hole. Interested readers are referred to this review [81] for more details. Together with the Einstein ring, the structure of the shadow can constrain the underlying parameters (e.g. charge, spin, mass) of the spacetime and, consequently, the parameters of the underlying theory [22–26] well as their

observational implications, have been investigated in recent times [27–30, 81–104]³.

Recently, a static black-bounce metric that can describe a black hole and a wormhole spacetime under suitable circumstances has been suggested in [105–108]. An interesting feature of this spacetime [105], is that it doesn't have a central singularity since an extra parameter has regularised it. This metric is not a solution to the vacuum Einstein equation. It requires the presence non-trivial energy-momentum tensor. The black-bounce spacetime has two different kinds of solutions depending on the choice of underlying regularisation parameters. When the solution does not admit any horizon, it corresponds to a Traversable wormhole solution. Otherwise, one can have a regular black hole solution without singularity (sometimes called a hidden wormhole), but there are two copies of it. Later, using the Newman-Janis algorithm, a rotating counterpart of this static black hole solution has been proposed in [107].

In recent times, the gravitational lensing in strong deflection limit and shadows for Schwarzschild and Reissner-Nordstrom black-bounce metrics separately have been investigated in [109–111]. Also, the strong deflection analysis for rotating black-bounce spacetime has been analyzed in [112] and the shadow of charged black-bounce metric has been analyzed in [113]. The weak lensing in the context of charged black-bounce metric has been investigated in [114]. In this paper, we consider the most general scenario by studying a charged rotating black-bounce metric [108]. First and foremost, we present an analytical computation of deflection angle for this charged black-bounce spacetimes, which has not been done. Then we consider the strong deflection limit and discuss the dependence of the radius of the Einstein ring on the charge and the regularisation parameter. Lastly, we compute various observable related to the shadow cast by this metric and discuss their dependence of them on the underlying parameters of the spacetime. Particularly motivated by the recent observation from EHT [19], using the size of the shadow one perhaps can constrain the charge of the underlying spacetime, we have investigated how the observables related to the shadow for this charged rotating black-bounce depends on the charge parameter.

In this paper, we investigated the general setup that is possible. The article is organized as follows. In Sec. (2), we review the null geodesics in a charged, rotating black-bounce spacetime(also known as Kerr-Newman black-bounce spacetime) and find out the turning point of light rays and how it depends on the impact parameter. We also investigate the

³This list is by no means exhaustive. Interested readers are referred to this review [81] and citations there for more details.

critical impact parameter and the innermost circular orbit in this section. In the Sec. (3), we give a general perturbative method to calculate the equatorial deflection angle. Next, in Sec. (4), we briefly consider the strong deflection analysis of equatorial lensing. In Sec. (5), we discuss some observational signatures and their dependence on charge and regularisation parameters in a strong deflection limit. In Sec (6) we discuss the strong lensing in the non-equatorial plane at small inclination and comment on the caustic structure. Finally, we discuss observable quantities related to shadow size, their dependence on charge and regularisation parameters, and the implications of our results in Sec. (7). In Sec. (8), we give concluding remarks. Some necessary mathematical details are given in the Appendix (A). Also, we have set the value of the speed of light c and Newton's gravitational constant G to unity.

2 Null geodesics in the Kerr-Newman black-bounce spacetime

We briefly discuss the null geodesics in Kerr-Newman black-bounce spacetime. In Boyer-Lindquist coordinate the line element can be written as [108],

$$\begin{aligned} ds^2 &= g_{\mu\nu} dx^\mu dx^\nu \\ &= -\frac{\Delta}{\rho^2} (a \sin^2 \theta d\phi - dt)^2 + \frac{\sin^2 \theta}{\rho^2} ((r^2 + a^2 + l^2) d\phi - a dt)^2 + \rho^2 \left(\frac{dr^2}{\Delta} + d\theta^2 \right) \end{aligned} \quad (2.1)$$

where

$$\rho^2 = r^2 + l^2 + a^2 \cos^2 \theta, \Delta(r) = (r^2 + a^2 + l^2) - 2m\sqrt{r^2 + l^2} + Q^2. \quad (2.2)$$

In (2.1) and (2.2), $m \geq 0$ is the ADM mass, Q is the charge of the black hole, $a = \frac{J}{m}$ is the angular momentum per unit mass and $l > 0$ is the extra parameter that is the cause of the non-existence of the central singularity. Note that in this case, the range of the radial coordinate is $-\infty < r < \infty$. The Kerr-Newman black-bounce metric reduces to the Kerr metric by taking $Q = 0, l = 0$. The event horizon can be found by equating $\Delta(r) = 0$ and is given by,

$$R_H = \sqrt{\left[\left(m + \sqrt{m^2 - (a^2 + Q^2)} \right)^2 - l^2 \right]} \quad (2.3)$$

along with the reality condition $m^2 - (a^2 + Q^2) > 0$ and $m + \sqrt{m^2 - (a^2 + Q^2)} > l$. The lagrangian for photon is given by,

$$\mathcal{L} = \frac{1}{2} g_{\mu\nu} \dot{x}^\mu \dot{x}^\nu \quad (2.4)$$

where the four-velocity, $\dot{x}^\mu = \frac{dx^\mu}{d\lambda}$, is defined in terms of some convenient parameter $\tilde{\lambda}$.

Light rays travels along null geodesic obeying the condition $\dot{x}^\mu \dot{x}_\mu = 0$. As the consequences of the fact that the Kerr-Newman black-bounce spacetime is independent of time t and azimuthal coordinate ϕ , there exists two associated killing vectors $\xi_t^\mu = (1, 0, 0, 0)$ and $\xi_\phi^\mu = (0, 0, 0, 1)$. The associated conserved quantities are: $E = -\xi_t^\mu \dot{x}_\mu$ and $L = \xi_\phi^\mu \dot{x}_\mu$. Additionally there exists a Carter constant \mathcal{K} coming from the separability of Hamilton-Jacobi equation and is given by,

$$\mathcal{K} = \dot{x}_\mu \dot{x}_\nu K^{\mu\nu} - (L - a E)^2. \quad (2.5)$$

The spacetime under consideration admits a non trivial Killing tensor,

$$K^{\mu\nu} = \Delta(r) l^\mu n^\nu + r^2 g^{\mu\nu}, \quad (2.6)$$

where the tetrads l^μ and n^μ mentioned below.

$$\begin{aligned} l^\mu &= \frac{1}{\Delta(r)} \left[(r^2 + a^2 + l^2) \delta_t^\mu + \Delta(r) \delta_r^\mu + a \delta_\phi^\mu \right], \\ n^\mu &= \frac{1}{\Delta(r)} \left[(r^2 + a^2 + l^2) \delta_t^\mu - \Delta(r) \delta_r^\mu + a \delta_\phi^\mu \right]. \end{aligned} \quad (2.7)$$

Using these three constants of motion and a convenient choice of parameter the null geodesic equations can be described by the following four first order differential equation,

$$\begin{aligned} \rho^4 \dot{r}^2 &= ((r^2 + l^2 + a^2) E - a L)^2 - \Delta(r) ((L - a E)^2 + \mathcal{K}) := R^2(r), \\ \rho^2 \dot{\phi} &= - \left(a E - \frac{L}{\sin^2 \theta} \right) + \frac{a [E(r^2 + a^2 + l^2) - a L]}{\Delta}, \\ \rho^2 \dot{t} &= -a (a E \sin^2 \theta - L) + \frac{(r^2 + a^2 + l^2) [E(r^2 + a^2 + l^2) - a L]}{\Delta}, \\ \rho^4 \dot{\theta}^2 &= \mathcal{K} + \cos^2 \theta \left(a^2 E^2 - \frac{L^2}{\sin^2 \theta} \right) := \Theta(\theta)^2. \end{aligned} \quad (2.8)$$

In (2.8) the dot stands for the derivative with respect to $\tilde{\lambda}$. Subsequently, for simplicity we restrict ourselves to the equatorial plane i.e, $\theta = \frac{\pi}{2}, \dot{\theta} = 0$ and $\mathcal{K} = 0$. Now we can rewrite the radial geodesic equation as,

$$\frac{\dot{r}^2}{L^2} + V(r) = \frac{1}{\lambda^2}, \lambda = \frac{L}{E} \quad (2.9)$$

where the effective potential $V(r)$ is defined as,

$$V(r) = \frac{1}{r^2 + l^2} \left[1 - \frac{a^2}{\lambda^2} + \left(1 - \frac{a}{\lambda} \right)^2 \left(-\frac{2m}{\sqrt{r^2 + l^2}} + \frac{Q^2}{r^2 + l^2} \right) \right]. \quad (2.10)$$

λ is the impact parameter. One can get a clear idea about the nature of the potential from the Fig. 1. The equation (2.9) is mimicking the motion of a particle in the effective potential

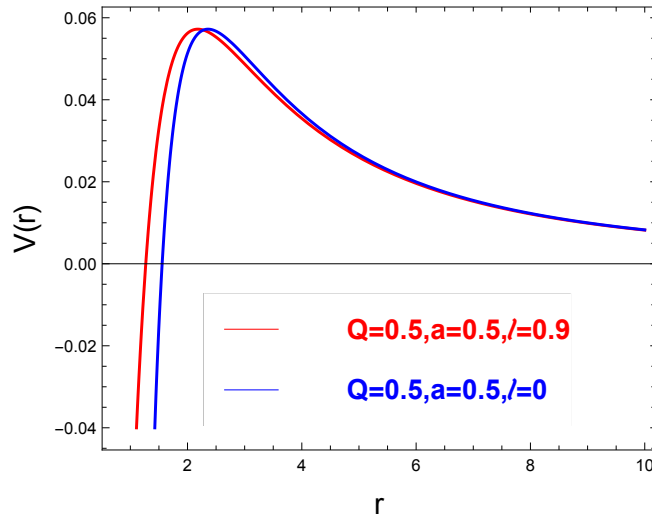


Figure 1: The red and blue curves represent the effective potential $V(r)$ for Kerr-Newman black-bounce and Kerr-Newman spacetime respectively. For large values l , we can see that the maxima of $V(r)$ shifts towards left i.e the radius of photon sphere (r_c) becomes smaller.

$V(r)$. By taking appropriate limits (2.9) reduces to corresponding well-known equations for the Kerr ($l = 0, Q = 0$) and Schwarzschild black hole ($l = Q = a = 0$) respectively. Note that, for Kerr-Newman black hole ($l = 0$), the charge Q gives a repulsive effect to the light rays. This repulsive effect prevents the light rays fall into the black hole. However, for this black-bounce metric, the regularisation parameter l provides an extra attractive effect to the light rays.

Now consider light rays that start from infinity and approach to the black hole, and then turn back to the infinity to reach the observer. These light rays will have radial turning

point namely, the closest approach to the black hole r_0 , determined by,

$$\left(\frac{\dot{r}^2}{L^2}\right)\Big|_{r=r_0} = \frac{1}{\lambda^2} - V(r_0) = 0. \quad (2.11)$$

From (2.11) we get,

$$\tilde{r}_0^4 - \lambda^2 \left(1 - \frac{a^2}{\lambda^2}\right) \tilde{r}_0^2 + 2m\lambda^2 \left(1 - \frac{a}{\lambda}\right)^2 \tilde{r}_0 = Q^2 \lambda^2 \left(1 - \frac{a}{\lambda}\right)^2 \quad (2.12)$$

where, $\tilde{r}_0 = \sqrt{r_0^2 + l^2}$.

Then solving (2.11) we get,

$$r_0(\lambda) = \left(\frac{\lambda}{\sqrt{6}} \sqrt{1 - \omega^2} \left[\sqrt{1 + \hat{\gamma}} + \sqrt{2 - \hat{\gamma} - \frac{3\sqrt{6}m(1 - \omega)^2}{\lambda(1 - \omega^2)^{3/2} \sqrt{1 + \hat{\gamma}}}} \right]^2 - l^2\right)^{1/2} \quad (2.13)$$

where $\omega, \chi, \rho, \hat{\gamma}$ are given by,

$$\begin{aligned} \omega &= \frac{a}{\lambda}, \quad \rho = \frac{12Q^2}{\lambda^2(1 + \omega)^2}, \quad \hat{\gamma} = \sqrt{1 - \rho} \cos\left(\frac{2\chi}{3}\right), \\ \chi &= \arccos\left(\frac{3\sqrt{3}m(1 - \omega)^2}{\lambda(1 - \omega^2)^{3/2}(1 - \rho)^{3/4}} \sqrt{1 - \frac{\lambda^2(1 + \omega)^3}{54m^2(1 - \omega)} [1 + 3\rho - (1 - \rho)^{3/2}]}\right). \end{aligned} \quad (2.14)$$

Eq. (2.13) reduces to that of Kerr-Newmann for $l = 0$. As evident from Fig. (2), the additional attractive effect because of l pulls the distance of closest approach r_0 . As can be seen from Fig. (2), for a fixed impact parameter λ , r_0 is smaller for the rotating charged black-bounce metric compared to that of its Kerr-Newman counterpart. From Fig. (2), it is also evident that the non zero charge Q gives an additional repulsive effect on the light rays.

Critical impact parameter and the photon sphere:

We end this section by discussing the position of the photon sphere and the critical impact parameter for the light rays coming from asymptotic infinity. This will be useful for the analysis of deflection in the subsequent sections. From Fig.(1) we can see that the effective potential $V(r)$ in (2.10) vanishes at infinity and *attain maximum value at the $r = r_c$* . This critical radius r_c is the radius of the radius of photon sphere. This is defined by the following

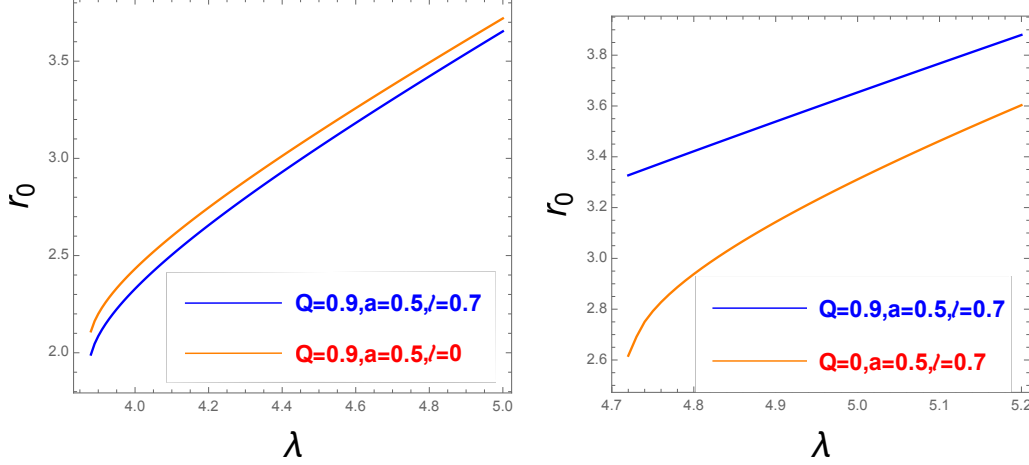


Figure 2: Variation of the distance of closest approach r_0 with respect to the impact parameter λ for different choices of black hole parameters. The left one shows the variation of r_0 with respect to λ for different regularisation parameters (l). The right one shows the variation of r_0 with respect to λ for different charge parameters (Q).

condition,

$$\left. \frac{\partial V(r)}{\partial r} \right|_{r=r_c} = 0. \quad (2.15)$$

From (2.15) we can find out

$$r_c(\lambda_c) = \sqrt{\left(\frac{3m\hat{\zeta}}{2} \left[1 + \sqrt{1-\zeta} \right] \right)^2 - l^2} \quad (2.16)$$

where,

$$\tilde{r} = \sqrt{r^2 + l^2}, \quad \hat{\zeta} = \left(\frac{1 - \frac{a}{\lambda_c}}{1 + \frac{a}{\lambda_c}} \right), \quad \zeta = \frac{8Q^2}{9m^2} \hat{\zeta}.$$

One can easily check that the result presented in (2.16) can be reduced to that of Kerr-Newmann black holes black hole in limit $l = 0$.

Note that the turning point of the photon is r_0 defined in (2.13) attains its minimum value at r_c . The corresponding value of the impact parameter is defined as λ_c . If for some λ , r_0 becomes less than r_c then the photon will be captured by the black hole. Hence λ_c is known as the critical impact parameter. Finally, substituting equation (2.13) into (2.16) we can write $\lambda_c = \lambda_c(a, Q, l)$ and $r_c = r_c(a, Q, l)$.

3 Computation of deflection angle: Analytical approach

The study of gravitational lensing has been very important in recent days because it has a direct consequence on the observational appearances of the black holes [7]. In this section, we will present some analytical results for deflection angle for photon passing near a Kerr-Newman black-bounce spacetime. This is one of the main goals of this paper. The first task is to calculate the deflection angle of the photon in some preferred plane. For simplicity we choose the equatorial plane, i.e, $\theta = \frac{\pi}{2}$ and $\dot{\theta} = 0$. In order to study the lensing of light rays by a black hole spacetime, we need to take a strong deflection limit, i.e. when the turning point of photon r_0 is very close to the radius of photon sphere r_c . We can do it in two different ways: first, calculate the exact deflection angle and take the strong deflection limit or take the strong deflection limit from the beginning and arrive at the formula for the deflection angle. In this section, we give an analytical calculation of the exact deflection angle in perturbative order. In the next section, we adopt the second approach, calculate the deflection angle in the strong deflection limit, and discuss its observational consequences.

To calculate the deflection angle we will follow the method of [115,116]. Before proceeding with the computation we define the following coordinate,

$$u := \frac{1}{\sqrt{r^2 + l^2}}. \quad (3.1)$$

Then combining the first two equations in (2.8) we get,

$$\left(\frac{du}{d\phi}\right)^2 = \left(\frac{du}{dr} \frac{dr}{d\phi}\right)^2 = \frac{r^2}{(r^2 + l^2)^3} \frac{\dot{r}^2}{\dot{\phi}^2} = (u^4 - l^2 u^6) \frac{\dot{r}^2}{\dot{\phi}^2}. \quad (3.2)$$

Now our goal is to rewrite the \dot{r} and $\dot{\phi}$ as function of u . We have,

$$\begin{aligned} \dot{r}^2 &= L^2 \left(\frac{1}{\lambda^2} - V(r) \right) \\ &= L^2 \left[\frac{1}{\lambda^2} - \left[\frac{1}{r^2 + l^2} \left(1 - \frac{a^2}{\lambda^2} + \left(1 - \frac{a}{\lambda} \right)^2 \left(-\frac{2m}{\sqrt{r^2 + l^2}} + \frac{Q^2}{r^2 + l^2} \right) \right) \right] \right] \\ &= L^2 \left[\frac{1}{\lambda^2} - u^2 \left(1 - \frac{a^2}{\lambda^2} \right) - Q^2 \left(1 - \frac{a}{\lambda} \right)^2 u^4 + 2m \left(1 - \frac{a}{\lambda} \right)^2 u^3 \right] := L^2 B(u). \end{aligned} \quad (3.3)$$

Now mimicking the same procedure we can write,

$$\begin{aligned}
\dot{\phi}^2 &= \frac{1}{(r^2 + l^2)^2} \left[- (a E - L) + \frac{a[(E(r^2 + a^2 + l^2)) - aL]}{r^2 + a^2 + l^2 - 2m\sqrt{r^2 + l^2} + Q^2} \right]^2 \\
&= \frac{1}{u^4} \left[E \lambda \left(1 - \frac{a}{\lambda} \right) + \frac{a E (1 + a^2 u^2 - a u^2 \lambda)}{1 + a^2 u^2 - 2mu + Q^2 u^2} \right]^2 \\
&= \frac{L^2}{u^4} \left[\frac{1 - (2mu - Q^2 u^2)(1 - \frac{a}{\lambda})}{1 - 2mu + (a^2 + Q^2)u^2} \right]^2.
\end{aligned} \tag{3.4}$$

Combining equation (3.3) and (3.4) and using the equation (3.2) we get,

$$\left(\frac{du}{d\phi} \right)^2 = (1 - l^2 u^2) \left[\frac{1 - 2mu + (a^2 + Q^2)u^2}{1 - (2mu - Q^2 u^2)(1 - \frac{a}{\lambda})} \right]^2 B(u). \tag{3.5}$$

The deflection angle of the photon $\hat{\alpha}$ can be calculated by integrating the equation (3.5) over u from 0 to $\frac{1}{\sqrt{r_0^2 + l^2}}$, where r_0 is the turning point and then evaluating the resulting expression at the critical value r_c [40],

$$\hat{\alpha} = -\pi + 2 \int_0^{\frac{1}{\sqrt{r_0^2 + l^2}}} \frac{1}{\sqrt{1 - l^2 u^2}} \left[\frac{1 - (2mu - Q^2 u^2)(1 - \frac{a}{\lambda})}{1 - 2mu + (a^2 + Q^2)u^2} \right] \frac{1}{\sqrt{B(u)}}. \tag{3.6}$$

In (3.6), the polynomial $B(u)(1 - l^2 u^2)$ is of *degree six*. Hence we can not write this integral as a complete form of elliptic integral. However to make some progress analytically we will assume

$$l^2 u^2 \ll 1. \tag{3.7}$$

Then we can Taylor expand $\frac{1}{\sqrt{1 - l^2 u^2}} = 1 + \frac{l^2 u^2}{2} + \mathcal{O}(l^4 u^4)$. Therefore we can rewrite (3.6) upto $\mathcal{O}(l^4)$,

$$\begin{aligned}
\hat{\alpha} &= -\pi + 2 \int_0^{\frac{1}{\sqrt{r_0^2 + l^2}}} du \left(1 + \frac{l^2 u^2}{2} \right) \left[\frac{1 - (2mu - Q^2 u^2)(1 - \omega)}{1 - 2mu + (a^2 + Q^2)u^2} \right] \frac{1}{\sqrt{B(u)}} + \mathcal{O}(l^4) \\
&= \hat{\alpha}_{\text{KN}} + l^2 * (\text{correction term}) + \mathcal{O}(l^4) \\
&= \hat{\alpha}_{\text{KN}} \Big|_{\sqrt{r_0^2 + l^2}} + l^2 * \xi(m, a, \lambda, Q) + \mathcal{O}(l^4).
\end{aligned} \tag{3.8}$$

$\hat{\alpha}_{\text{KN}}$ corresponds to the deflection angle for Kerr-Newman black hole which can be obtained

from (3.8) in $l = 0$ limit and

$$\xi(m, a, \lambda, Q) = \int_0^{\frac{1}{\sqrt{r_0^2 + l^2}}} u^2 \left[\frac{1 - (2mu - Q^2 u^2)(1 - \omega)}{1 - 2mu + (a^2 + Q^2)u^2} \right] \frac{1}{\sqrt{B(u)}} du, \quad (3.9)$$

with $\omega = \frac{a}{\lambda}$. We now rewrite $B(u)$ as,

$$B(u) = -Q^2(1 - w)^2(u - u_1)(u - u_2)(u - u_3)(u - u_4), \quad (3.10)$$

where the roots are defined as,

$$u_1 = \frac{X_1 - 2m - X_2}{4m\sqrt{r_0^2 + l^2}}, \quad (3.11)$$

$$u_2 = \frac{1}{\sqrt{r_0^2 + l^2}}, \quad (3.12)$$

$$u_3 = \frac{X_1 - 2m + X_2}{4m\sqrt{r_0^2 + l^2}}, \quad (3.13)$$

$$u_4 = \frac{2m}{Q^2} - \frac{X_1}{2m\sqrt{r_0^2 + l^2}}. \quad (3.14)$$

By suitably choosing the constants X_1 and X_2 allows us to write down the roots in the following order $u_1 < u_2 < u_3 < u_4$. Among them u_2, u_3, u_4 are positive roots while u_1 is a negative root. In order to extract the roots, we need to substitute equations (3.11) to (3.14) into (3.10) and comparing it with the coefficients of u^0, u^2, u^3, u^4 in (3.3) we will get [116],

$$\begin{aligned} Q^2 \left[X_2^2 - (X_1 - 2m)(X_1 + 6m) + 4X_1^2 \right] &= 16m^2 \sqrt{r_0^2 + l^2} \left(X_1 - \sqrt{r_0^2 + l^2} \frac{1 + \omega}{1 - \omega} \right), \\ X_2^2 - (X_1^2 - 2m)^2 &= \frac{8m(X_1 - 2m)(Q^2 X_1 - 4m^2 \sqrt{r_0^2 + l^2})}{Q^2(X_1 - 2m) - 4m^2 \sqrt{r_0^2 + l^2}}, \\ \left[X_2^2 - (X_1^2 - 2m)^2 \right] &\left(\frac{1}{8m(r_0^2 + l^2)^{\frac{3}{2}}} - \frac{Q^2 X_1}{32m^3(r_0^2 + l^2)^2} \right) = \frac{1}{\lambda^2(1 - \omega)^2}. \end{aligned} \quad (3.15)$$

Combining the first and second equation of (3.15) gives the equation for X_1 , which is given

by,

$$\begin{aligned} & \frac{Q^2}{2m} X_1^3 - \left(Q^2 + 4m\sqrt{r_0^2 + l^2} \right) X_1^2 + \left(4m^2\sqrt{r_0^2 + l^2} + 2mQ^2 + \frac{8m^3(r_0^2 + l^2)}{Q^2} + \frac{2m((r_0^2 + l^2)(1 + \omega))}{(1 - \omega)} \right) X_1 \\ & = 4m^2 Q^2 + \frac{4m^2(r_0^2 + l^2)(1 + \omega)}{(1 - \omega)} + \frac{8m^2(r_0^2 + l^2)^{\frac{3}{2}}(1 + \omega)}{Q^2(1 - \omega)}. \end{aligned} \quad (3.16)$$

We can analytically solve the equation(3.16) and the positive real root is given by,

$$X_1(m, Q, \omega, l, r_0) = \frac{2m(Q^2 + 4m\sqrt{r_0^2 + l^2})}{3Q^2} + \frac{8m^2\sqrt{r_0^2 + l^2}}{3Q^2} \sqrt{1 + \frac{Q^2}{2m^2} \left(\frac{m}{\sqrt{r_0^2 + l^2}} - \frac{3(1 + \omega)}{2(1 - \omega)} - \frac{Q^2}{r_0^2 + l^2} \right)} \cos \left(\frac{\delta}{3} + \frac{2\pi}{3} \right). \quad (3.17)$$

where,

$$\delta = \arccos \left(\frac{-8m^3(r_0^2 + l^2)^{3/2} - 3mQ^2(r_0^2 + l^2) \left(2m - \frac{3\sqrt{r_0^2 + l^2}(1 + \omega)}{(1 - \omega)} \right) - 3Q^4\sqrt{r_0^2 + l^2} \left(5m - \frac{3\sqrt{r_0^2 + l^2}(1 + \omega)}{(1 - \omega)} \right) + 10Q^6}{\left[4m^2(r_0^2 + l^2) + Q^2\sqrt{r_0^2 + l^2} \left(2m - \frac{3\sqrt{r_0^2 + l^2}(1 + \omega)}{(1 - \omega)} \right) - 2Q^4 \right]^{3/2}} \right). \quad (3.18)$$

At this point, we can check that in the limit $Q = 0, l = 0$, δ becomes π . Then (3.18) can be written as,

$$X_1(m, \omega, Q = 0, l = 0, r_0) = r_0 \frac{1 + \omega}{1 - \omega}. \quad (3.19)$$

This is exactly the result for Kerr black hole [115]. For Reissner-Nordstrom black hole we have $a = 0, l = 0$ and the roots of the equation (3.16) then reduces to,

$$X_1(m, Q, \omega = 1, l = 0, r_c) = 2m \left(\frac{2mr_0}{Q^2} - 1 \right) \Big|_{r_c} \quad (3.20)$$

where r_c is defined in (2.16) and the result (3.20) matches with the known result [116].

Now we turn our attention to the function mentioned inside the third bracket of (3.9). Let

$$F(u) = 1 - 2mu + (a^2 + Q^2)u^2 = (u - u_-)(u - u_+), \quad (3.21)$$

where u_- and u_+ are the roots of the equation $F(u)$. Therefore we can rewrite the following term in the manner described below.

$$\frac{1 - 2mu(1 - \omega) + Q^2u^2(1 - \omega)}{1 - 2mu + (a^2 + Q^2)u^2} = \frac{K_+}{u_+ - u} + \frac{K_-}{u_- - u} + \frac{K_{Q+}u}{u_+ - u} + \frac{K_{Q-}u}{u_- - u} \quad (3.22)$$

where,

$$u_{\pm} = \frac{m \pm \sqrt{m^2 - (a^2 + Q^2)}}{a^2 + Q^2}. \quad (3.23)$$

As evident from (3.23) u_{\pm} are positive. Solving equation (3.22), we can find out the constants K_- , K_+ , K_{Q+} , K_{Q-} and given by,

$$K_+ = \frac{2m(1 - \omega) \left(m + \sqrt{m^2 - (a^2 + Q^2)} \right) - (a^2 + Q^2)}{2(a^2 + Q^2) \sqrt{m^2 - (a^2 + Q^2)}}, \quad (3.24)$$

$$K_- = \frac{(a^2 + Q^2) - 2m(1 - \omega) \left(m - \sqrt{m^2 - (a^2 + Q^2)} \right)}{2(a^2 + Q^2) \sqrt{m^2 - (a^2 + Q^2)}}, \quad (3.25)$$

$$K_{Q+} = \frac{-Q^2(1 - \omega) \left(m + \sqrt{m^2 - (a^2 + Q^2)} \right)}{2(a^2 + Q^2) \sqrt{m^2 - (a^2 + Q^2)}}, \quad (3.26)$$

$$K_{Q-} = \frac{Q^2(1 - \omega) \left(m - \sqrt{m^2 - (a^2 + Q^2)} \right)}{2(a^2 + Q^2) \sqrt{m^2 - (a^2 + Q^2)}}. \quad (3.27)$$

Finally integral in (3.9) can be written as,

$$\begin{aligned} \xi(m, a, \lambda, Q) &= \int_0^{u_2} du u^2 \left[\frac{K_+}{u_+ - u} + \frac{K_-}{u_- - u} + \frac{K_{Q+}u}{u_+ - u} + \frac{K_{Q-}u}{u_- - u} \right] \frac{1}{\sqrt{-Q^2(1-\omega)^2(u-u_1)(u-u_2)(u-u_3)(u-u_4)}} \\ &= K_+ g(u_+ \Delta \mathbf{F} + [(u_1 - u_4) \Delta \Pi(\alpha^2) + u_4 \Delta \mathbf{F}] - u_+^2 \frac{1}{(u_+ - u_1)} \left[\frac{u_1 - u_4}{u_+ - u_4} \Delta \Pi(\alpha_{+3}^2) + \frac{u_+ - u_1}{u_+ - u_4} \Delta \mathbf{F} \right]) \\ &+ K_- g(u_- \Delta \mathbf{F} + [(u_1 - u_4) \Delta \Pi(\alpha^2) + u_4 \Delta \mathbf{F}] - u_-^2 \frac{1}{(u_- - u_1)} \left[\frac{u_1 - u_4}{u_- - u_4} \Delta \Pi(\alpha_{-3}^2) + \frac{u_- - u_1}{u_- - u_4} \Delta \mathbf{F} \right]) \\ &+ K_{Q+} g \left[(u_+^2 - 2u_+u_4 + u_+^2 - \frac{u_+^3}{u_+ - u_4}) \Delta \mathbf{F} + (u_+(u_1 - u_4) - \frac{u_+^3(u_1 - u_4)}{(u_+ - u_1)(u_+ - u_4)}) \Delta \Pi(\alpha_{+3}^2) \right. \\ &\left. - 2u_4(u_1 - u_4) \mathbf{V}_1(\alpha^2) - (u_1 - u_4)^2 \mathbf{V}_2(\alpha^2) \right] + K_{Q-} g \left[(u_-^2 - 2u_-u_4 + u_-^2 - \frac{u_-^3}{u_- - u_4}) \Delta \mathbf{F} \right. \\ &\left. + (u_-(u_1 - u_4) - \frac{u_-^3(u_1 - u_4)}{(u_- - u_1)(u_- - u_4)}) \Delta \Pi(\alpha_{-3}^2) - 2u_4(u_1 - u_4) \mathbf{V}_1(\alpha^2) - (u_1 - u_4)^2 \mathbf{V}_2(\alpha^2) \right] \end{aligned} \quad (3.28)$$

where,

$$\begin{aligned}\Delta \mathbf{F} &= F(\phi, k) - F\left(\frac{\pi}{2}, k\right), \quad \Delta \mathbf{\Pi}(\alpha^2) = \mathbf{\Pi}(\phi, \alpha^2, k) - \mathbf{\Pi}\left(\frac{\pi}{2}, \alpha^2, k\right), \\ \Delta \mathbf{\Pi}(\alpha_{\pm 3}^2) &= \mathbf{\Pi}(\phi, \alpha_{\pm 3}^2, k) - \mathbf{\Pi}\left(\frac{\pi}{2}, \alpha_{\pm 3}^2, k\right)\end{aligned}\tag{3.29}$$

and, \mathbf{V}_1 and \mathbf{V}_2 is given by,

$$\begin{aligned}\mathbf{V}_1(\alpha^2) &= \mathbf{\Pi}\left(\frac{\pi}{2}, \alpha^2, k\right) - \mathbf{\Pi}(\phi, \alpha^2, k), \\ \mathbf{V}_2(\alpha^2) &= \frac{1}{2(\alpha^2 - 1)(k^2 - \alpha^2)} \left[\alpha^2 \left(E\left(\frac{\pi}{2}, k\right) - E(\phi, k) \right) + (k^2 - \alpha^2) \left(F\left(\frac{\pi}{2}, k\right) - F(\phi, k) \right) \right], \\ &\left(2\alpha^2 k^2 + 2\alpha^2 - \alpha^4 - 3k^2 \right) \left(\mathbf{\Pi}\left(\frac{\pi}{2}, \alpha^2, k\right) - \mathbf{\Pi}(\phi, \alpha^2, k) \right) - \frac{\alpha^4 \sin \phi \sqrt{1 - \sin^2 \phi} \sqrt{1 - k^2 \sin^2 \phi}}{1 - \alpha^2 \sin^2 \phi} \end{aligned}\tag{3.30}$$

and

$$\begin{aligned}g &= \frac{2}{\sqrt{Q^2(1 - \omega)^2(u_4 - u_2)(u_3 - u_1)}}, \quad \alpha^2 = \frac{u_1 - u_2}{u_4 - u_2} < 0, \quad \alpha_{\pm 3}^2 = \alpha^2 \frac{u_{\pm} - u_4}{u_{\pm} - u_1}, \\ k^2 &= \frac{(u_4 - u_3)(u_2 - u_1)}{(u_4 - u_2)(u_3 - u_1)}, \quad \phi = \arcsin \sqrt{\frac{(X_2 + 2m - X_1)[4m^2 \sqrt{r_0^2 + l^2} - Q^2(X_1 + 2m)]}{(X_2 + 6m - X_1)(4m^2 \sqrt{r_0^2 + l^2} - Q^2 X_1)}}.\end{aligned}\tag{3.31}$$

Note that, $\mathbf{\Pi}(\phi, \alpha^2, k)$ and $\mathbf{\Pi}\left(\frac{\pi}{2}, \alpha^2, k\right)$ are the incomplete and complete elliptic integral of third kind respectively. Also, $F(\phi, k)$ and $F\left(\frac{\pi}{2}, k\right)$ are the incomplete and complete elliptic integral of first kind. Additionally, in $\mathbf{V}_{1,2}$ we have $E(\phi, k)$ and $E\left(\frac{\pi}{2}, k\right)$, which are incomplete and complete elliptic integral of second kind respectively. The details of the computation are given in the Appendix (A).

Together with (3.8), (3.28) provides an expression of equatorial deflection angle for Kerr-Newman black-bounce metric upto $\mathcal{O}(l^2)$. This result is one of the main results of the paper.

4 Strong deflection analysis of equatorial lensing

To get further insight into the deflection angle for our context and make contact with the possible observational signature, in this section, we study the strong deflection limit [40] of

the equatorial deflection angle ($\theta = \frac{\pi}{2}$) of the light rays mentioned in the previous section. It is difficult to take the strong deflection limit of (3.28) directly. It will be easier to take the strong field limit of the integrand of (3.6) first and then do the integration. As mentioned before, we will only consider those light rays whose turning point is very close to the radius of photon sphere.

On the equatorial plane the metric takes the following form,

$$ds^2 = -\mathcal{A}(r)dt^2 + \mathcal{B}(r)dr^2 + \mathcal{C}(r)d\phi^2 - \mathcal{D}(r)dt d\phi \quad (4.1)$$

with

$$\begin{aligned} \mathcal{A}(r) &= \frac{1}{\rho^2}(\Delta(r) - a^2), \quad \mathcal{B}(r) = \frac{\rho^2}{\Delta}, \quad \mathcal{C}(r) = \frac{1}{\rho^2} \left[(r^2 + a^2 + l^2)^2 - \Delta(r)a^2 \right], \\ \mathcal{D}(r) &= \frac{2}{\rho^2} \left[(r^2 + a^2 + l^2)a - \Delta(r)a \right]. \end{aligned} \quad (4.2)$$

Note that all metric components are evaluated at equatorial plane. We have already seen that due to the existing symmetries, the spacetime admits two conserved quantities E and L . For the sake of simplicity we set $E = 1$. Therefore the impact parameter $\lambda = L$. From (2.9), after using the fact that at the distance of closest approach $r = r_0$ and $\dot{r} = 0$, we get the following,

$$\begin{aligned} L &= \frac{-\mathcal{D}_0 + \sqrt{4\mathcal{A}_0\mathcal{C}_0 + \mathcal{D}_0^2}}{2\mathcal{A}_0} \\ &= \frac{\sqrt{l^2 + r_0^2} \left((l^2 + r_0^2) \sqrt{a^2 - 2m\sqrt{l^2 + r_0^2} + l^2 + Q^2 + r_0^2} + a \left(Q^2 - 2m\sqrt{l^2 + r_0^2} \right) \right)}{Q^2\sqrt{l^2 + r_0^2} + l^2 \left(\sqrt{l^2 + r_0^2} - 2m \right) + r_0^2 \left(\sqrt{l^2 + r_0^2} - 2m \right)}. \end{aligned} \quad (4.3)$$

The subscript “0” denotes functions are evaluated at $r = r_0$. From the equation of motion of ϕ (the second equation of (2.8)) we get,

$$\phi(r_0) = 2 \int_{r_0}^{\infty} \frac{\sqrt{\mathcal{B}\mathcal{A}_0}(\mathcal{D} + 2L\mathcal{A})}{\sqrt{4\mathcal{A}\mathcal{C} + \mathcal{D}^2} \sqrt{\mathcal{C}\mathcal{A}_0 - \mathcal{A}\mathcal{C}_0 + L(\mathcal{A}\mathcal{D}_0 - \mathcal{D}\mathcal{A}_0)}} dr. \quad (4.4)$$

In the strong field limit, we consider only those photons whose distance of closest approach $r_0 \approx r_c$, where r_c is the radius of the photon sphere. Hence the deflection angle α (3.6)

can be expanded in terms of r_c or equivalently the critical impact parameter λ_c . When the distance of the closest approach r_0 is greater than r_c , the light rays get deflected (but it can orbit around the black hole several times before reaching the observer). Otherwise, around $r = r_c$, $\hat{\alpha}$ diverges and the photon gets absorbed by the black hole. Following the method developed here [38, 40], one can find out the nature of the divergence in the deflection angle when the photons are very close to the radius of photon sphere $r = r_c$. One can define two variables y, z as,

$$y = \mathcal{A}(r), z = \frac{y - y_0}{1 - y_0}. \quad (4.5)$$

Now one can express azimuthal angle defined in (4.4) in terms of these two new variables,

$$\phi(r_0) = \int_0^1 \mathcal{R}(z, r_0) \mathcal{F}(z, r_0) dz \quad (4.6)$$

where,

$$\mathcal{R}(z, r_0) = \frac{2(1 - y_0) \sqrt{\mathcal{B}\mathcal{A}_0} (\mathcal{D} + 2LA)}{A' \sqrt{4\mathcal{A}\mathcal{C}^2 + \mathcal{C}\mathcal{D}^2}} \quad (4.7)$$

$$\mathcal{F}(z, r_0) = \frac{1}{\sqrt{\frac{1}{\mathcal{C}}(\mathcal{C}\mathcal{A}_0 - \mathcal{A}\mathcal{C}_0 + L(\mathcal{A}\mathcal{D}_0 - \mathcal{D}\mathcal{A}_0))}} = \frac{1}{\sqrt{\mathcal{H}}}, \quad (4.8)$$

$$\mathcal{H} = \frac{1}{\mathcal{C}}(\mathcal{C}\mathcal{A}_0 - \mathcal{A}\mathcal{C}_0 + L(\mathcal{A}\mathcal{D}_0 - \mathcal{D}\mathcal{A}_0)). \quad (4.9)$$

One can see that the function $\mathcal{R}(z, r_0)$ is regular for any values of z and r_0 but the function $\mathcal{F}(z, r_0)$ is divergent for $z = 0$, i.e at $r = r_0$. Therefore one can rewrite (4.4) after extracting the divergent part,

$$\phi(r_0) = \phi_{\mathcal{R}}(r_0) + \phi_{\mathcal{F}}(r_0) \quad (4.10)$$

where the divergent part can be written as,

$$\phi_{\mathcal{F}}(r_0) = \int_0^1 \mathcal{R}(z = 0, r_c) \mathcal{F}_0(z, r_0) dz. \quad (4.11)$$

As we know, at $r_0 = r_c$ the deflection angle should diverge, signalling that the black hole captures the photon. Then our goal is to find out the nature of the divergence. We can find out the nature of the divergence by investigating the denominator (4.6). With the aim of

doing so we Taylor expand the denominator of $\mathcal{F}_0(r_0, z)$ (4.12) around $z = 0$.

$$\mathcal{F}_0(z, r_0) \approx \frac{1}{\sqrt{\gamma_1(r_0)z + \gamma_2(r_0)z^2 + \mathcal{O}(z^3)}}. \quad (4.12)$$

Note that, if $\gamma_1(r_0) = 0$, (this happens when r_0 coincides with the radius of photon sphere [117]) then it is evident from (4.12), the leading term goes as $\frac{1}{z}$ in small z limit. Hence after the integration will give a logarithmic divergence as shown in (4.21). To identify γ_1 and γ_2 we first Taylor expand \mathcal{H} defined in (4.9).

$$\mathcal{H}(z, r_0) = \mathcal{H}(0, r_0) + \left. \frac{\partial \mathcal{H}}{\partial z} \right|_{z=0} z + \frac{1}{2!} \left. \frac{\partial^2 \mathcal{H}}{\partial z^2} \right|_{z=0} z^2 + \mathcal{O}(z^3), \text{ with } \mathcal{H}(0, r_0) = 0. \quad (4.13)$$

Therefore using (4.8) we can identify γ_1 and γ_2 as ,

$$\begin{aligned} \gamma_1 &:= \left. \frac{\partial \mathcal{H}}{\partial z} \right|_{z=0} \\ &= \frac{1 - \mathcal{A}_0}{\mathcal{A}'_0 \mathcal{C}_0} \left(\mathcal{A}_0 \mathcal{C}'_0 - \mathcal{A}'_0 \mathcal{C}_0 - L(\mathcal{A}_0 \mathcal{D}'_0 - \mathcal{A}'_0 \mathcal{D}_0) \right) \end{aligned} \quad (4.14)$$

and

$$\begin{aligned} \gamma_2 &:= \left. \frac{1}{2!} \frac{\partial^2 \mathcal{H}}{\partial z^2} \right|_{z=0} \\ &= \frac{(1 - \mathcal{A}_0)^2}{2\mathcal{C}_0^2 \mathcal{A}_0^3} \left[2\mathcal{C}_0 \mathcal{C}'_0 \mathcal{A}_0'^2 + (\mathcal{C}_0 \mathcal{C}_0'' - 2\mathcal{C}_0'^2) \mathcal{A}_0 \mathcal{A}'_0 - \mathcal{C}_0 \mathcal{C}'_0 \mathcal{A}_0 \mathcal{A}_0'' \right. \\ &\quad \left. + L(\mathcal{A}_0 \mathcal{C}_0 (\mathcal{A}_0'' \mathcal{D}'_0 - \mathcal{A}'_0 \mathcal{D}_0'') + 2\mathcal{A}'_0 \mathcal{C}'_0 (\mathcal{A}_0 \mathcal{D}'_0 - \mathcal{A}'_0 \mathcal{D}_0)) \right]. \end{aligned} \quad (4.15)$$

The regular part can be written as,

$$\phi_{\mathcal{R}}(r_0) = \int_0^1 \mathcal{G}(z, r_0) dz \quad (4.16)$$

where $\mathcal{G}(z, r_0) = \mathcal{R}(z, r_0) \mathcal{F}(z, r_0) - \mathcal{R}(z = 0, r_c) \mathcal{F}_0(z, r_0)$. As we discussed the coefficient $\gamma_1 = 0$. This implies,

$$\mathcal{A}_0 \mathcal{C}'_0 - \mathcal{A}'_0 \mathcal{C}_0 - L(\mathcal{A}_0 \mathcal{D}'_0 - \mathcal{A}'_0 \mathcal{D}_0) \Big|_{r_0=r_c} = 0. \quad (4.17)$$

From (4.17) we get,

$$2a^2 \left(Q^2 - \sqrt{l^2 + r_c^2} \right) + 2a \left(\sqrt{l^2 + r_c^2} - Q^2 \right) \sqrt{a^2 - 2\sqrt{l^2 + r_c^2} + l^2 + Q^2 + r_c^2 + l^4 + l^2 \left(-5\sqrt{l^2 + r_c^2} + 3Q^2 + 2r_c^2 + 6 \right) - 7Q^2\sqrt{l^2 + r_c^2} - 5r_c^2\sqrt{l^2 + r_c^2} + 2Q^4 + 3(Q^2 + 2)r_c^2 + r_c^4} = 0 \quad (4.18)$$

It can be easily checked that, using the expression for critical impact parameter λ_c as mentioned in (4.3), one gets the same expression for the radius of photon sphere as mentioned in (2.16). So we can say that (4.18) gives yet another definition of the photon sphere. For more details on the geometry of photon spheres and various complementary definitions of photon spheres, interested readers are referred [117].

For Kerr-Newman black-bounce spacetime, we can numerically find out the radius of the photon sphere for fixed values of l, Q, a . The variation of photon sphere radius with respect to the different black hole parameters is shown in Figure(3). We can clearly see from Fig.(3), that for fixed values of l and a as Q increases the radius of photon sphere r_c decreases. Even r_c decreases if we fix any two parameters and increase the other parameter.

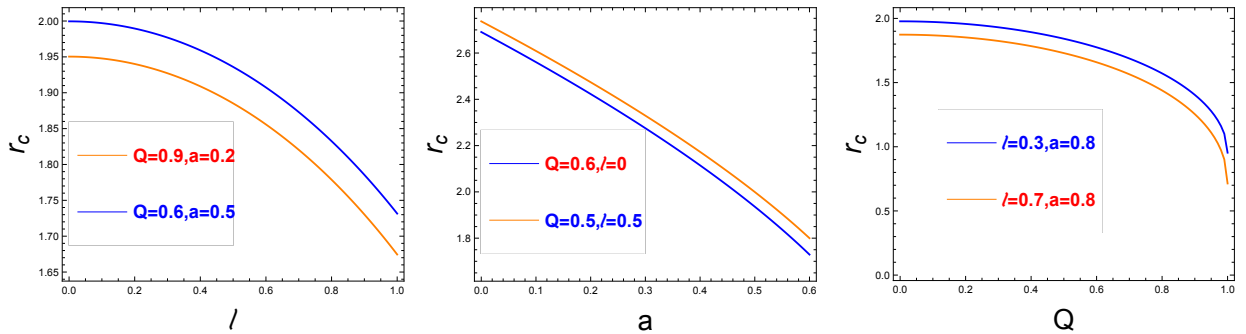


Figure 3: Plots showing radii of photon sphere for charged, rotating Kerr-Newman black-bounce metric for different values of black hole parameters. Left most figure displays the variation of photon sphere with respect to l for fixed a and Q . The middle figure shows the variation of photon sphere with respect to a for fixed l and Q and the right most figure shows the variation of photon sphere with respect to Q for fixed a and l .

Armed with these we can now evaluate the divergent integral (4.11),

$$\begin{aligned}
\phi_{\mathcal{F}}(r_0 \approx r_c) &= \mathcal{R}(z=0, r_c) \int_0^1 \frac{1}{\sqrt{\gamma_1 z + \gamma_2 z^2}} dz \\
&= \mathcal{R}(z=0, r_0 \approx r_c) \frac{2}{\sqrt{\gamma_2}} \operatorname{arcsinh} \left(\sqrt{\frac{\gamma_2}{\gamma_1}} \right) \\
&= \mathcal{R}(z=0, r_0 \approx r_c) \frac{2}{\sqrt{\gamma_2}} \log \left(\frac{\sqrt{\gamma_2} + \sqrt{\gamma_2 + \gamma_1}}{\sqrt{\gamma_1}} \right). \tag{4.19}
\end{aligned}$$

We know that $\phi_{\mathcal{F}}(r_0)$ diverges at $r_0 = r_c$ i.e, when the coefficient $\gamma_1 = 0$. So the idea is to expand the $\gamma_1(r_0)$ around $r_0 = r_c$ upto first order and substitute it into (4.19) in order to get the nature of $\phi_{\mathcal{F}}(r_0 \approx r_c)$.

$$\begin{aligned}
\gamma_1(r_0) &= \left. \frac{\partial \gamma_1}{\partial r_0} \right|_{r_0=r_c} (r_0 - r_c) + \mathcal{O}(r_0 - r_c)^2, \\
\gamma_2(r_0) &= \gamma_2(r_c) + \left. \frac{\partial \gamma_2}{\partial r_0} \right|_{r_0=r_c} (r_0 - r_c) + \mathcal{O}(r_0 - r_c)^2. \tag{4.20}
\end{aligned}$$

Substituting (4.20) into (4.19) and using the condition (4.17) we get,

$$\phi_{\mathcal{F}}(r_0 \approx r_c) = -\tilde{a} \log \left(\frac{r_0}{r_c} - 1 \right) + \tilde{b} + \mathcal{O}(r_0 - r_c). \tag{4.21}$$

Alternatively, one can write the equation (4.21) in terms of impact parameter as [40],

$$\hat{\alpha}(\lambda) = -\bar{a} \log \left(\frac{\lambda}{\lambda_c} - 1 \right) + \bar{b} + \mathcal{O}(\lambda - \lambda_c), \tag{4.22}$$

where the coefficients are,

$$\bar{a} = \sqrt{\frac{2\mathcal{A}_c \mathcal{B}_c}{\mathcal{A}_c \mathcal{C}_c'' - \mathcal{A}_c'' \mathcal{C}_c + \lambda_c (\mathcal{A}_c'' \mathcal{D}_c - \mathcal{A}_c \mathcal{D}_c'')}} , \tag{4.23}$$

$$\bar{b} = -\pi + b_R + \bar{a} \log \left(\frac{4\gamma_{2c} \mathcal{C}_c}{\lambda_c \mathcal{A}_c (\mathcal{D}_c + 2\lambda_c \mathcal{A}_c)} \right), \tag{4.24}$$

$$\lambda_c = L_c. \tag{4.25}$$

The variation of the deflection angle (4.22) with respect to the impact parameter is shown in Fig.(4). From the Fig. (4) we can see that, for non zero Q and l deflection angle $\hat{\alpha}(\lambda)$ for a fixed impact parameter decreases.

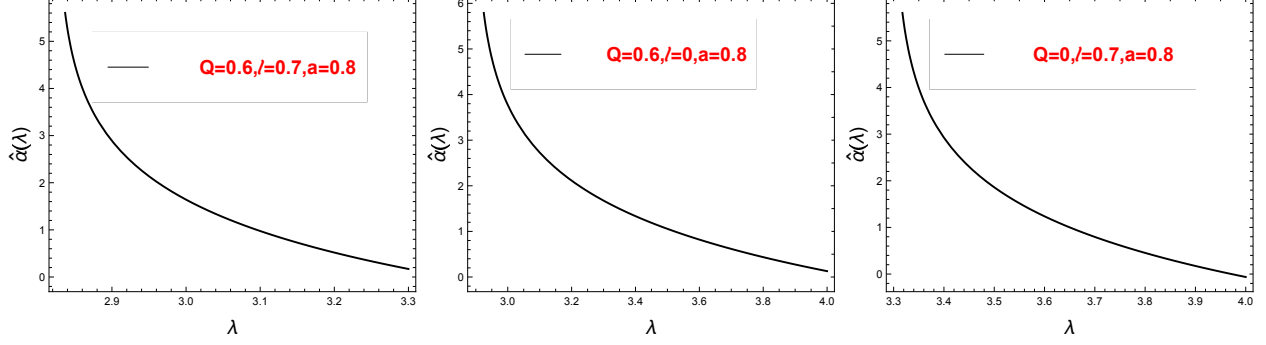


Figure 4: Plots showing the variation of the deflection angle $\hat{\alpha}$ with respect to the impact parameter λ for fixed values of black hole parameters Q, l, a .

The black hole can be thought of as a lens as gravitational field of which is curving the path of the photons. Let the angular separation between image and lens is $\theta = \frac{\lambda}{D_{ol}}$, where D_{ol} is the distance between the lens and the observer. Then the expression for the deflection angle (4.22) can be written as,

$$\hat{\alpha}(\theta) = -\bar{a} \log\left(\frac{\theta D_{ol}}{\lambda_c} - 1\right) + \bar{b} + \mathcal{O}(\lambda - \lambda_c) \quad (4.26)$$

where $b_R = \phi_{\mathcal{R}}(r_c) = \int_0^1 \mathcal{G}(z, r_c) dz$.

In order to do the integral we can expand $\mathcal{R}(z, r_c)$ around $z = 0$ and then putting it in (4.11). Formally we get the following expression,

$$b_R = \frac{1}{\sqrt{\gamma_2}} \int_0^1 \left(\frac{\mathcal{R}(z)}{z} - \frac{\mathcal{R}(0)}{z} \right) dz \Bigg|_{r_c} = \frac{1}{\sqrt{\gamma_2}} \sum_{n=1}^{\infty} \frac{1}{n} \frac{\partial^n \mathcal{R}}{\partial z^n} \Bigg|_{z=0} \rightarrow \text{finite}. \quad (4.27)$$

When the deflection angle is greater than 2π we will have multiple images of the source. Using the strong field deflection angle formula given in (4.26) and the lens equation, we can derive the angular radius of the Einstein ring, which is created due to the symmetric lensing of light rays coming from some distant source [118, 119]. In the next section, we will discuss the observational signatures of deflection angle.

5 Observational signatures in strong deflection limit

After providing theoretical analysis, in this we will discuss some aspects of observational signatures of deflection angle. The idea is to find the relation between deflection angle and the angular radius of the images (Einstein ring) using lens equation. In this paper we will use the following lens equation given in [120],

$$\beta = \theta - \frac{D_{LS}}{D_{OS}} \Delta\alpha_n \quad (5.1)$$

where $D_{OS} = D_{OL} + D_{LS}$, β is the angular separation between the source and the lens, and D_{LS}, D_{OS}, D_{OL} are the distances between lens to source, observer to source and observer to lens respectively and $\Delta\alpha_n = \hat{\alpha}(\theta) - 2n\pi$. Now we can write the angular separation between the lens and the n^{th} image as, $\theta_n = \theta_n^0 + \Delta\theta_n$, where θ_n^0 is the angular separation between the image and the lens when the extra deflection angle ($\Delta\theta_n$) over $2n\pi$ is negligible.

For the perfect alignment i.e, when $\beta = 0$ and assuming $\Delta\theta_n \ll \theta_n^0$, the angular separation (angular radius) can be written as [40],

$$\theta_n^{Einstein} = \frac{\lambda_c}{D_{OL}} \left[1 + \exp\left(\frac{\bar{b}}{\bar{a}} - \frac{2n\pi}{\bar{a}}\right) \right]. \quad (5.2)$$

$n = 1$ corresponds to the outermost Einstein ring. We plot some of these rings for different values of Q, a and l in Fig. (5).

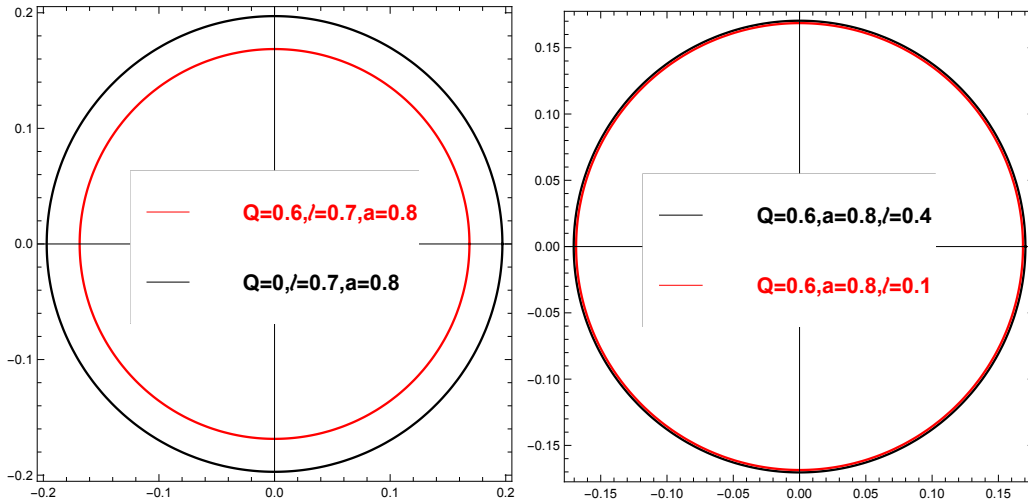


Figure 5: Polar plots showing the angular radius θ_1 for different Q, l, a values.

Angular separation		Percentage change	Values of Charge	Fixed parameters	
$\theta_1^{(1)}(Q_2)$	$\theta_1^{(2)}(Q_1)$	$\Delta\theta = \frac{(\theta_1^{(2)} - \theta_1^{(1)})}{\theta_1^{(1)}} \times 100$	(Q_1, Q_2)	l	a
0.1686	0.1970	16.9013	(0, 0.6)	0.7	0.8
0.18548	0.21590	16.399	(0.6, 0.8)	0.4	0.5
0.215903	0.232365	7.62463	(0.4, 0.6)	0.4	0.5

Table 1: Percentage change of the angular radius of first Einstein ring for different values of charge Q for fixed a and l .

Angular separation		Percentage change	Values of regularization parameter
$\theta_1^{(1)}(l_1)$	$\theta_1^{(2)}(l_2)$	$\Delta\theta = \frac{(\theta_1^{(2)} - \theta_1^{(1)})}{\theta_1^{(1)}} \times 100$	(l_1, l_2)
0.16856	0.1703	1.07059	(0.2, 0.4)
0.16856	0.16860	0.0186897	(0.2, 0.7)
0.168565	0.168568	0.001963	(0.1, 0.2)

Table 2: Percentage change of the angular radius of first Einstein ring for different values of regularisation parameter l for $a = 0.8$ and $Q = 0.6$.

From the Fig. (5) we can easily see (from the left-most plot in Fig. (5) that *as the charge of the black hole Q increases (for fixed values of l and a) the size of the ring decreases. On the other hand, the effect of change of l (for fixed value of a and Q) on the ring radius is negligible* as can be easily seen from the right-most plot in Fig. (5). To make this observation more concrete, we further make a comparative study as shown in the Table (1) and (2). We have listed some representative values of the percentage change of the angular radius of the outermost Einstein rings with respect to Q (for fixed a and l) and l (for fixed a and Q) in Table (1) and (2) respectively. These values corroborate perfectly the conclusion drawn above. We can conclude that, in future detections, if one able to resolve angular separation of various Einstein rings, then that will give us constraint on the charge of the underlying black-bounce metric.

6 Strong deflection analysis of non-equatorial lensing

In Section 5, we have investigated the lensing in the equatorial plane. In this section, we will further extend our study for the non-equatorial lensing at a small inclination to get a complete picture, as there is no spherical symmetry for the metric under consideration. We will follow [40] closely to carry out the analysis. In case of equatorial lensing we only need the one-dimensional lens equation. However, to investigate the caustic structure and magnification for non equatorial case, we need a two-dimensional lens equation given in [40]. We assume that inclination is $\theta = \frac{\pi}{2} - \psi$, where ψ is very small.

For non-equatorial plane we can not set the carter constant \mathcal{K} to 0 i.e, $\mathcal{K} \neq 0$. Rather for the small inward inclination angle we can write down the constants in terms of inclination angle ψ as follows,

$$L \approx \lambda \tag{6.1}$$

$$\mathcal{K} \approx h^2 + (\lambda^2 - a^2)\psi_0^2, \text{ with } \psi_0 \approx \frac{h}{\lambda} \tag{6.2}$$

Now using the θ and ϕ geodesic equation in 2.8 and requiring ψ to be small we will have,

$$\frac{d\psi}{d\phi} = \omega(r(\phi))\sqrt{\hat{\psi}^2 - \psi^2}, \text{ with } \hat{\psi} = \sqrt{\frac{h^2}{\lambda^2 - a^2} + \psi_0^2} \tag{6.3}$$

We are interested in the quantity (deflection angle),

$$\bar{\phi}_f = \int_0^{\phi_f} d\phi \omega(\phi) \tag{6.4}$$

where ϕ_f is the total azimuthal shift. Then the deflection angle can be written as

$$\bar{\phi}_f = 2 \int_{r_0}^{\infty} dr \omega(r) \frac{d\phi}{dr} = \int_0^1 dz \omega(r(z)) \mathcal{R}(z, r_0) \mathcal{F}(z, r_0) \tag{6.5}$$

where,

$$\omega(r) = \bar{\lambda} \frac{a^2 + \sqrt{r^2 + l^2}(\sqrt{r^2 + l^2} - 2)}{\sqrt{r^2 + l^2} \left(2a + \lambda(\sqrt{r^2 + l^2} - 2) \right) + Q^2(\lambda - a)} \tag{6.6}$$

with, $\bar{\lambda} = \sqrt{\lambda^2 - a^2}$. We can follow the same method to get the divergent nature of the

deflection angle as the function $\omega(r)$ is free of singularities and is given by,

$$\bar{\phi}_f = -\hat{a} \log \left(\frac{\lambda}{\lambda_c} - 1 \right) + \hat{b}. \quad (6.7)$$

Here,

$$\hat{a} = \frac{\omega(z=0, r_c) \mathcal{R}(z=0, r_c)}{2\sqrt{\gamma_{2c}}}, \quad (6.8)$$

$$\hat{b} = -\pi + \hat{b}_R + \hat{a} \log \left(\frac{4\gamma_{2c} \mathcal{C}_c}{\lambda_c \mathcal{A}_c (\mathcal{D}_c + 2\lambda_c \mathcal{A}_c)} \right), \quad (6.9)$$

where,

$$\hat{b}_R = \int_0^1 dz [\omega(z, r_c) \mathcal{R}(z, r_c) \mathcal{F}(z, r_c) - \omega(z=0, r_c) \mathcal{R}(z=0, r_c) \mathcal{F}(z, r_c)]. \quad (6.10)$$

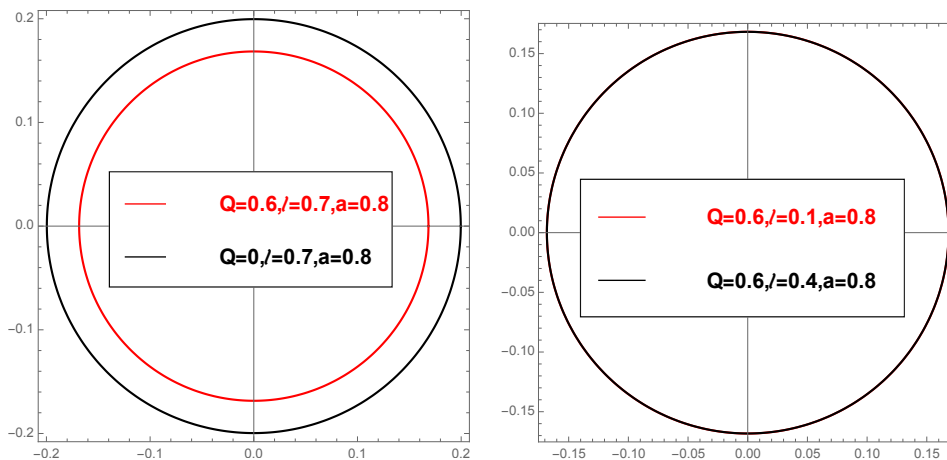


Figure 6: Polar plots showing the angular radius θ_1 for different Q, l, a values.

Fig (6) shows that the angular radius of first Einstein ring depends on the charge parameter of the black bounce metric considerably but the dependence on the regularisation parameter is minimal as we see in case of equatorial lensing.

Our interest is to find the position of the caustics, where the magnification diverges, and is given by [40], $\bar{\gamma}_k = -\bar{b} + \bar{a}(\hat{b} - k\pi)$. Here k is a positive integer. For each values of k , we have one caustic for the direct photon and one for the retrograde photon. For $k = 1$, we will find the caustic point in the weak field limit and for $k \geq 1$ corresponds to the strong field limit, and we are interested in this regime. In Table (3), we investigate the variation of the

(l, a)	Q	$\bar{\gamma}_2$
(0.4,0.5)	0.5	-6.62
(0.4,0.5)	0.6	-5.10
(0.4,0.5)	0.7	-0.16
(0.4,-0.5)	0.5	-5.69
(0.4,-0.5)	0.6	-5.84
(0.4,-0.5)	0.7	-5.90

Table 3: Angular position of the second caustic point for different charge parameter Q . The first three entities are for direct photon and the last three are for retrograde photon.

(Q, a)	l	$\bar{\gamma}_2$
(0.5,0.5)	0.4	-6.62
(0.5,0.5)	0.5	-6.68
(0.5,0.5)	0.6	-6.72
(0.5,-0.5)	0.7	-5.92
(0.5,-0.5)	0.8	-5.98
(0.5,-0.5)	1.0	-6.20

Table 4: Angular position of the second caustic point for different regularisation parameter l . The first three entities are for direct photons, and the last three are for retrograde photons.

second caustic point with respect to Q for fixed l and a . In Table (4), we investigate the variation of the second caustic point with respect to l for fixed Q and a . Comparing Table (3) and (4) we can conclude that the change of caustic points for different Q and different l is not that robust.

7 Analysis of the observables for the shadow

To complement our discussions in the previous section, we also investigate the size of shadow cast by the underlying spacetime and various associated observable quantities and their dependence on the charge of the black-bounce metric. In light of recent EHT observations, particularly as it is expected that the presence of charge affects the size of the shadow contour significantly [19].

For this, we first need to find out the region of unstable spherical light rays that acts as a boundary beyond which the photons will be captured by the black hole. This then leads to a black patch as no light rays reach the observer's line of sight and serve as the boundary

of the black patch, which is the so-called black hole shadow. Sometimes they are also called as photon spheres. For rotating black holes there are two circular photon orbits and the region between them is called the photon region. The photon region can be found by solving $\dot{r} = \ddot{r} = 0$. From equation (2.8) we get,

$$0 = \mathcal{R}(r) := \frac{R(r)}{E^2} = [(r^2 + a^2 + l^2) - a\lambda]^2 - \Delta(r)[\eta + (\lambda - a)^2] \quad \text{and}, \quad (7.1)$$

$$0 = \mathcal{R}'(r) = 4r[(r^2 + a^2 + l^2) - a\lambda] - \Delta'(r)[\eta + (\lambda - a)^2]. \quad (7.2)$$

where, $\lambda = \frac{L}{E}$ and $\eta = \frac{\mathcal{K}}{E^2}$. Now solving (7.1) and (7.2) we find the two constants λ and η and are given by,

$$\lambda = \left. \frac{(a^2 + l^2 + r^2)\Delta'(r) - 4r\Delta(r)}{a\Delta'(r)} \right|_{r=r_p} \quad (7.3)$$

and

$$\eta = \left. \frac{16a^2r^2\Delta(r) - l^4\Delta'(r)^2 - 2l^2r^2\Delta'(r)^2 + 8l^2r\Delta(r)\Delta'(r) - r^4\Delta'(r)^2 + 8r^3\Delta(r)\Delta'(r) - 16r^2\Delta(r)^2}{a^2\Delta'(r)^2} \right|_{r=r_p}. \quad (7.4)$$

Now substituting (7.3) and (7.4) in the positivity condition of the θ equation of motion (2.8) we will get the photon region,

$$\tilde{\mathcal{H}} : \eta + \cos^2\theta \left(a^2 - \frac{\lambda^2}{\sin^2\theta} \right) \Big|_{r=r_p} \geq 0 \quad (7.5)$$

$\tilde{\mathcal{H}}$ denotes the photon region and r_p denotes the values of radial coordinate r on the shadow contour.

In order to investigate the shadow structure we can define two asymptotic celestial coordinate at a given inclination angle θ_0 as [121],

$$\begin{aligned} \alpha &= -\lambda \csc(\theta_0) \\ \beta &= \pm \sqrt{\eta + a^2 \cos^2(\theta_0) - \lambda^2 \cot^2(\theta_0)} \end{aligned} \quad (7.6)$$

For simplicity we take $\theta_0 = \frac{\pi}{2}$. Then the coordinates become,

$$\alpha(r_p) = -\lambda(r_p), \quad \beta(r_p) = \pm \sqrt{\eta(r_p)} \quad (7.7)$$

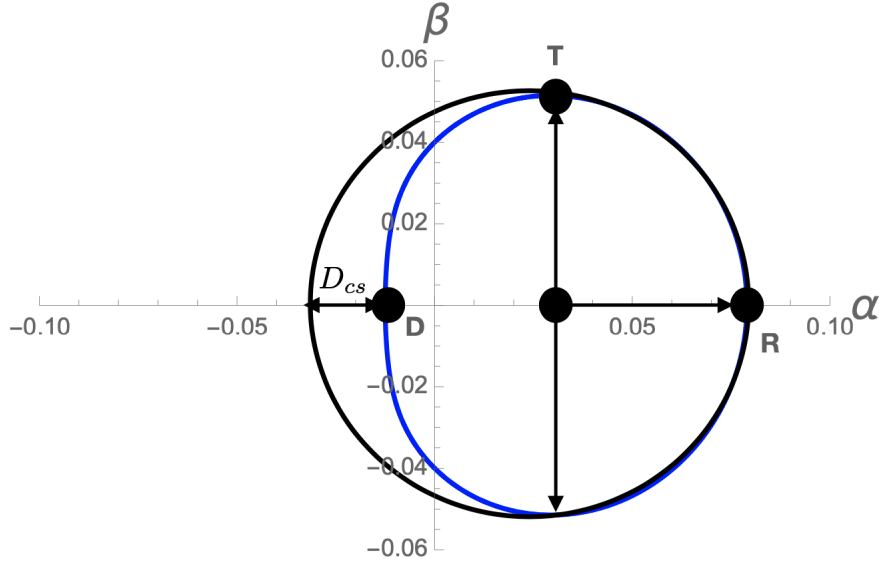


Figure 7: Figure displays various characteristic points on a typical shadow contour

Next, to analyze the effect of charge on the topology of the shadow contour, we compute the observable quantities [121]. Particularly we focus on the radius of the shadow and the distortion parameter. In order to investigate these, we first consider three characteristic points of the shadow contour as shown in Fig. (7). We follow the analysis of [121]. In order to find the Top (‘**T**’) point, we need to find the root of,

$$(\partial_{r_p}\beta)\Big|_{\theta_0=\frac{\pi}{2}} = 0 \implies (\partial_{r_p}\eta)\Big|_{\theta_0=\frac{\pi}{2}} = 0. \quad (7.8)$$

At **T**, β takes the maximum value. The condition (7.8) gives,

$$\begin{aligned} & \left(a^2 \left(\sqrt{l^2 + r_p^2} (2Q^2 + r_p^2) + l^2 \left(\sqrt{l^2 + r_p^2} \right. \right. \right. \\ & \left. \left. \left. - 3 \right) - 3r_p^2 \right) - l^6 + 2Q^4 \sqrt{l^2 + r_p^2} + l^2 \left(Q^2 \left(7\sqrt{l^2 + r_p^2} - 4r_p^2 - 9 \right) \right. \right. \\ & \left. \left. + 9\sqrt{l^2 + r_p^2} - 3r_p^2 \left(-4\sqrt{l^2 + r_p^2} + r_p^2 + 8 \right) \right) + 7Q^2 r_p^2 \sqrt{l^2 + r_p^2} + 9r_p^2 \sqrt{l^2 + r_p^2} + 6r_p^4 \sqrt{l^2 + r_p^2} \right. \\ & \left. + l^4 \left(6\sqrt{l^2 + r_p^2} - 2(Q^2 + 6) - 3r_p^2 \right) - 2(Q^2 + 6)r_p^4 - 9Q^2 r_p^2 - r_p^6 \right) = 0. \end{aligned} \quad (7.9)$$

We denote the solution of r corresponding to the point **T** coming from (7.9) by \tilde{r}_p .

Q	R_s	$\delta_s = \frac{D_{cs}}{R_s}$	$(\alpha_R - \alpha_D)$
0	5.196	0.03038	10.2344
0.1	5.1874	0.03072	10.2156
0.2	5.16124	0.03177	10.1585
0.3	5.11679	0.03369	10.0612
0.4	5.05298	0.0367677	9.92017
0.5	4.96791	0.0415804	9.72926
0.6	4.85869	0.0493605	9.72657
0.7	4.72068	0.0631616	9.1432
0.8	4.54599	0.0939478	8.66489

Table 5: The above table shows how the shadow distortion parameter changes with charge Q for $a = 0.5$ and $l = 0.6$.

To find the coordinates of other two points \mathbf{D} and \mathbf{R} we need to set $\beta = 0$ as evident from Fig. (6). The two real positive roots (r_p^+, r_p^-) of it characterize these two points \mathbf{D} and \mathbf{R} are respectively. So we have the following,

$$T : = \left(\alpha_T(\tilde{r}_p), \beta_T(\tilde{r}_p) \right)$$

$$R : = \left(\alpha(r_p^+), 0 \right) \tag{7.10}$$

$$D : = \left(\alpha(r_p^-), 0 \right) \tag{7.11}$$

For more details interested readers are referred [94, 121–123]. Further we compute two physical quantities namely [94, 121–123],

$$\text{Radius of the shadow: } R_s = \Delta\beta \tag{7.12}$$

where $\Delta\beta = \beta(\tilde{r}_p)$ and

$$\text{Distortion parameter: } \delta_s = \frac{D_{cs}}{R_s}, \quad D_{cs} = 2R_s - (\alpha_R - \alpha_D). \tag{7.13}$$

R_s is basically the radius of the reference circle as shown by the black curve in Fig (6) and D_{cs} measures the deviation from circularity when the shadow gets distorted whenever there are non-vanishing a . A typical distorted shadow contour is shown by blue curve in Fig. (6).

We can use these two quantities (R_s, δ_s) we can make contact with the observational data. We list values of these quantities in Table (5). As discussed before, we are particularly

interested in investigating the effect of charge on the size of the shadow contour. *It is evident from the data listed in Table (5) that, for fixed values of a and l as we increase the value of the charge Q the shadow becomes more distorted. From this analysis we can clearly see the effect of charge on the observational appearance of this black-bounce metric.*⁴ But the change in the distortion parameter δ_s as evident from the Table (5) is such that the EHT can not resolve this with its current resolution power [7]. But in the future, we hope that with the increase of resolution power, this change can be detected and help provide tighter constraints on the underlying parameter space.

8 Discussions

In summary, the motion of light rays around Kerr-Newman black-bounce spacetime has been studied in this paper. We first study the null geodesics and the innermost circular orbit in the bounce spacetime. From this investigation, we found that the black hole parameter l gives an extra attractive effect to the photon motion. Effectively the position of photon sphere has been pulled back in comparison with the Kerr-Newman black hole along with the repulsive effect caused by the charge of the black hole, which has a direct consequence on the observational appearance of the black hole. *We then give an analytical description of the equatorial deflection angle perturbatively in l , in terms of different kinds of elliptic integrals.* The non-zero l decreases the deflection angle for a fixed impact parameter. Our work gives a general methodology to study deflection angle analytically.

Throughout the paper, we give a comparative study of different observational signatures in Kerr-Newman black-bounce spacetime as well as a detailed analytical study. In this context, we first study the strong deflection analysis of the equatorial deflection angle, and this has direct observational consequences as this gives information about the Einstein rings. We conclude this analysis by investigating the first-order Einstein ring using the lens equation. From our analysis, we conclude that the size of the Einstein ring prominently depends on the black hole charge. *We observed that, as we decrease the charge (Q), the size of the ring increases. On the other hand, the effect of the regularisation parameter (l) on the ring radius is minimal compared to the effect of charge for a fixed value of spin parameter a . Furthermore, we also investigate the Einstein ring in case of small polar inclination. We observed that the*

⁴In principle, we can calculate the distortion parameter different inclination angles θ_0 , but that will not change the conclusion drawn in this section.

dependence on charge (Q) and regularisation parameter (l) remain the same as in the case of equatorial lensing. Also, we showed that the change in the position of caustic points with the change of charge (Q) and regularisation parameter (l) is not that considerable. One can apply this to different black hole spacetime to get an exact analytical expression.

Furthermore, motivated by the recent observations from EHT [19], we compute the distortion parameter for the shadow cast by this metric and investigate its dependence on the charge parameter Q to complement our analysis for the Einstein ring. We hope that these results will help us to effectively constrain the parameter space of this black-bounce metric in the near future with the increase of the resolving power of the telescope. Note that we have chosen the parameter space such that the horizon exists but it would be interesting to investigate the shadow structure when we do not have horizon and $r_p = r_{\text{throat}}$. In that case, there might be a possibility of getting a significant change in the distortion parameter quantifying the topology of the shadow due to the regularization parameter l [124].⁵

Several interesting avenues can be perused in future. Our work can be extended for other black-bounce spacetime e.g [125]. One can study multilevel images in this spacetime [126]. First of all, our analytical study presented in Sec. 3 requires a small l expansion and also, the study of non-equatorial lensing in Sec. 6 assumes a small inclination angle. It will be interesting to go beyond this regime, which will require a completely numerical study. We leave this investigation for future study. One can also study multilevel images in this spacetime [126]. From that analysis, one can predict how much precision of resolution is needed for distinguishing different Einstein rings. Apart from that, one can investigate strong gravitational lensing in an environment of thin accretion, or plasma [127]. Last but not least, another important quantity from the image analysis point of view that can be analysed is the two-point correlation function of intensity fluctuations on the photon ring, which arises due to the photon moving around multiple orbits around the central object. We hope to make a similar analysis for this black-bounce metric along the line of [128]. These studies will further help us to make contact with realistic astrophysical scenarios. We hope to report about some of these issues in the near future.

⁵We thank Naoki Tsukamoto for pointing out this reference.

Acknowledgements

A.B is supported by Start-Up Research Grant (SRG/2020/001380), Mathematical Research Impact Centric Support Grant (MTR/2021/000490) by the Department of Science and Technology Science and Engineering Research Board (India) and Relevant Research Project grant (202011BRE03RP06633-BRNS) by the Board Of Research In Nuclear Sciences (BRNS), Department of atomic Energy, India. Authors thank Abhishek Chowdhuri and Mostafizur Rahman for useful discussions.

A Appendix 1: Details of the integrals used in Section (3)

In this section we will show how to arrive the elliptic closed form of the integrals that is used in Section 3). We have encountered mainly two types of integral given by,

$$I_1 = \int_0^{u_2} du \frac{u^2}{(u - u_+) \sqrt{-(u - u_1)(u - u_2)(u - u_3)(u - u_4)}} \quad (\text{A.1})$$

and

$$I_2 := \int_0^{u_2} du \frac{u^3}{(u - u_+) \sqrt{-(u - u_1)(u - u_2)(u - u_3)(u - u_4)}} \quad (\text{A.2})$$

with $u_4 > u_3 > u_2 > 0 > u_1$.

We can write I_1 (defined in (A.1)) as,

$$\begin{aligned} I_1 &= \int_0^{u_2} du \frac{1}{\sqrt{-(u - u_1)(u - u_2)(u - u_3)(u - u_4)}} \left[u_+ + u + \frac{u_+^2}{u - u_+} \right] \\ &= \mathbf{N}_1 + \mathbf{N}_2 + \mathbf{N}_3, \end{aligned} \quad (\text{A.3})$$

where

$$\mathbf{N}_1 = \int_0^{u_2} du \frac{u_+}{\sqrt{-(u - u_1)(u - u_2)(u - u_3)(u - u_4)}} = u_+ g \left(F\left(\frac{\pi}{2}, k\right) - F(\phi, k) \right), \quad (\text{A.4})$$

$$\begin{aligned}
\mathbf{N}_2 &= \int_0^{u_2} du \frac{u}{\sqrt{-(u-u_1)(u-u_2)(u-u_3)(u-u_4)}} \\
&= \int_0^{u_1} du \frac{u}{\sqrt{-(u-u_1)(u-u_2)(u-u_3)(u-u_4)}} + \int_{u_1}^{u_2} du \frac{u}{\sqrt{-(u-u_1)(u-u_2)(u-u_3)(u-u_4)}} \\
&= -g u_1 \int_0^{t_1} dt \frac{1 - \frac{u_4 \alpha^2}{u_1} sn^2 t}{1 - \alpha^2 t} + g u_1 \int_0^{s_1} dt \frac{1 - \frac{u_4 \alpha^2}{u_1} sn^2 t}{1 - \alpha^2 t} \\
&= g u_1 \left[\left(1 - \frac{u_4}{u_1}\right) \left(\Pi\left(\frac{\pi}{2}, \alpha^2, k\right) - \Pi(\phi, \alpha^2, k) \right) + \frac{u_4}{u_1} \left(F\left(\frac{\pi}{2}, k\right) - F(\phi, k) \right) \right] \\
&= g \left[(u_1 - u_4) \left(\Pi\left(\frac{\pi}{2}, \alpha^2, k\right) - \Pi(\phi, \alpha^2, k) \right) + u_4 \left(F\left(\frac{\pi}{2}, k\right) - F(\phi, k) \right) \right]
\end{aligned} \tag{A.5}$$

and

$$\begin{aligned}
\mathbf{N}_3 &= \int_0^{u_2} du \frac{u_+^2}{(u-u_+) \sqrt{-(u-u_1)(u-u_2)(u-u_3)(u-u_4)}} \\
&= u_+^2 \frac{g}{(u_+ - u_1)} \left[\frac{u_1 - u_4}{u_+ - u_4} \left(\Pi(\phi, \alpha_3^2, k) - \Pi\left(\frac{\pi}{2}, \alpha_3^2, k\right) \right) + \frac{u_+ - u_1}{u_+ - u_4} \left(F(\phi, k) - F\left(\frac{\pi}{2}, k\right) \right) \right].
\end{aligned} \tag{A.6}$$

Finally we get,

$$\begin{aligned}
I_1 &= \int_0^{u_2} du \frac{u^2}{(u-u_+) \sqrt{-(u-u_1)(u-u_2)(u-u_3)(u-u_4)}} \\
&= u_+ g \left(F\left(\frac{\pi}{2}, k\right) - F(\phi, k) \right) + g \left[(u_1 - u_4) \left(\Pi\left(\frac{\pi}{2}, \alpha^2, k\right) - \Pi(\phi, \alpha^2, k) \right) + u_4 \left(F\left(\frac{\pi}{2}, k\right) - F(\phi, k) \right) \right] \\
&+ u_+^2 \frac{g}{(u_+ - u_1)} \left[\frac{u_1 - u_4}{u_+ - u_4} \left(\Pi(\phi, \alpha_3^2, k) - \Pi\left(\frac{\pi}{2}, \alpha_3^2, k\right) \right) + \frac{u_+ - u_1}{u_+ - u_4} \left(F(\phi, k) - F\left(\frac{\pi}{2}, k\right) \right) \right].
\end{aligned} \tag{A.7}$$

Next we focus on I_2 defined in (A.2).

$$\begin{aligned}
I_2 &= \int_0^{u_2} du \frac{u^3}{(u-u_+) \sqrt{-(u-u_1)(u-u_2)(u-u_3)(u-u_4)}} \\
&= \int_0^{u_2} du \frac{1}{\sqrt{-(u-u_1)(u-u_2)(u-u_3)(u-u_4)}} \left[(u-u_+)^2 + 3u_+ u + \frac{u_+^3}{u-u_+} \right] \\
&= \mathbf{M}_1 + \mathbf{M}_2 + \mathbf{M}_3.
\end{aligned} \tag{A.8}$$

Now we will again do the integrals piece-wise and get,

$$\begin{aligned}
\mathbf{M}_1 &= \int_0^{u_2} du \frac{u^2}{\sqrt{-(u-u_1)(u-u_2)(u-u_3)(u-u_4)}} - 2u_+ \int_0^{u_2} du \frac{u}{\sqrt{-(u-u_1)(u-u_2)(u-u_3)(u-u_4)}} \\
&+ \int_0^{u_2} \frac{du}{\sqrt{-(u-u_1)(u-u_2)(u-u_3)(u-u_4)}} \\
&= g \left[u_4^2 \left(F\left(\frac{\pi}{2}, k\right) - F(\phi, k) \right) + 2u_4(u_1 - u_4) \mathbf{V}_1 + (u_1 - u_4)^2 \mathbf{V}_2 \right] \\
&- 2u_+ g \left[(u_1 - u_4) \left(\Pi\left(\frac{\pi}{2}, \alpha^2, k\right) - \Pi(\phi, \alpha^2, k) \right) + u_4 \left(F\left(\frac{\pi}{2}, k\right) - F(\phi, k) \right) \right] \\
&+ u_+^2 g \left[F\left(\frac{\pi}{2}, k\right) - F(\phi, k) \right],
\end{aligned} \tag{A.9}$$

$$\begin{aligned}
\mathbf{M}_2 &= 3u_+ \int_0^{u_2} du \frac{u}{\sqrt{-(u-u_1)(u-u_2)(u-u_3)(u-u_4)}} \\
&= 3u_+ g \left[(u_1 - u_4) \left(\Pi\left(\frac{\pi}{2}, \alpha^2, k\right) - \Pi(\phi, \alpha^2, k) \right) + u_4 \left(F\left(\frac{\pi}{2}, k\right) - F(\phi, k) \right) \right],
\end{aligned} \tag{A.10}$$

and

$$\begin{aligned}
\mathbf{M}_3 &= u_+^3 \int_0^{u_2} du \frac{1}{(u-u_+) \sqrt{-(u-u_1)(u-u_2)(u-u_3)(u-u_4)}} \\
&= u_+^3 \frac{g}{(u_+ - u_1)} \left[\frac{u_1 - u_4}{u_+ - u_4} \left(\Pi(\phi, \alpha_3^2, k) - \Pi\left(\frac{\pi}{2}, \alpha_3^2, k\right) \right) + \frac{u_+ - u_1}{u_+ - u_4} \left(F(\phi, k) - F\left(\frac{\pi}{2}, k\right) \right) \right].
\end{aligned} \tag{A.11}$$

Therefore the integral I_2 can be written as,

$$\begin{aligned}
I_2 &= \int_0^{u_2} du \frac{u^3}{(u-u_+) \sqrt{-(u-u_1)(u-u_2)(u-u_3)(u-u_4)}} \\
&= g \left[\left(u_4^2 - 2u_+ u_4 + u_+^2 - \frac{u_+^3}{u_+ - u_4} \right) \left(F\left(\frac{\pi}{2}, k\right) - F(\phi, k) \right) \right. \\
&+ \left(u_+(u_1 - u_4) - \frac{u_+^3(u_1 - u_4)}{(u_+ - u_1)(u_+ - u_4)} \right) \left(\Pi\left(\frac{\pi}{2}, \alpha_3^2, k\right) - \Pi(\phi, \alpha_3^2, k) \right) \\
&\left. + 2u_4(u_1 - u_4) \mathbf{V}_1 + (u_1 - u_4)^2 \mathbf{V}_2 \right]
\end{aligned} \tag{A.12}$$

where \mathbf{V}_1 and \mathbf{V}_2 is given by,

$$\begin{aligned}\mathbf{V}_1 &= \Pi\left(\frac{\pi}{2}, \alpha^2, k\right) - \Pi(\phi, \alpha^2, k), \\ \mathbf{V}_2 &= \frac{1}{2(\alpha^2 - 1)(k^2 - \alpha^2)} \left[\alpha^2 \left(E\left(\frac{\pi}{2}, k\right) - E(\phi, k) \right) + (k^2 - \alpha^2) \left(F\left(\frac{\pi}{2}, k\right) - F(\phi, k) \right) \right], \\ & (2\alpha^2 k^2 + 2\alpha^2 - \alpha^4 - 3k^2) \left(\Pi\left(\frac{\pi}{2}, \alpha^2, k\right) - \Pi(\phi, \alpha^2, k) \right) - \frac{\alpha^4 \sin \phi \sqrt{1 - \sin^2 \phi} \sqrt{1 - k^2 \sin^2 \phi}}{1 - \alpha^2 \sin^2 \phi} \end{aligned} \quad (\text{A.13})$$

and

$$\begin{aligned}g &= \frac{2}{\sqrt{(u_4 - u_2)(u_3 - u_1)}}, \quad \alpha^2 = \frac{u_1 - u_2}{u_4 - u_2} < 0, \quad \alpha_3^2 = \alpha^2 \frac{u_+ - u_4}{u_+ - u_1}, \\ k^2 &= \frac{(u_4 - u_3)(u_2 - u_1)}{(u_4 - u_2)(u_3 - u_1)}, \quad \phi = \arcsin \sqrt{-\left(\frac{(u_4 - u_2)u_1}{(u_4 - u_1)u_4} \right)}. \end{aligned} \quad (\text{A.14})$$

References

- [1] **LIGO Scientific, Virgo** Collaboration, B. P. Abbott *et al.*, *Observation of Gravitational Waves from a Binary Black Hole Merger*, Phys. Rev. Lett. **116** (2016), no. 6, 061102 [1602.03837].
- [2] **LIGO Scientific, Virgo** Collaboration, B. P. Abbott *et al.*, *Properties of the Binary Black Hole Merger GW150914*, Phys. Rev. Lett. **116** (2016), no. 24, 241102 [1602.03840].
- [3] **LIGO Scientific, Virgo** Collaboration, B. P. Abbott *et al.*, *GW151226: Observation of Gravitational Waves from a 22-Solar-Mass Binary Black Hole Coalescence*, Phys. Rev. Lett. **116** (2016), no. 24, 241103 [1606.04855].
- [4] **LIGO Scientific, VIRGO** Collaboration, B. P. Abbott *et al.*, *GW170104: Observation of a 50-Solar-Mass Binary Black Hole Coalescence at Redshift 0.2*, Phys. Rev. Lett. **118** (2017), no. 22, 221101 [1706.01812], [Erratum: Phys.Rev.Lett. 121, 129901 (2018)].
- [5] **LIGO Scientific, KAGRA, VIRGO** Collaboration, R. Abbott *et al.*, *Observation of Gravitational Waves from Two Neutron Star–Black Hole Coalescences*, Astrophys. J. Lett. **915** (2021), no. 1, L5 [2106.15163].

- [6] **KAGRA** Collaboration, K. Kokeyama, *Observing the Universe from Underground Gravitational Wave Telescope KAGRA*, in *3rd World Summit on Exploring the Dark Side of the Universe*, pp. 41–48. 2020.
- [7] **Event Horizon Telescope** Collaboration, K. Akiyama *et al.*, *First M87 Event Horizon Telescope Results. I. The Shadow of the Supermassive Black Hole*, *Astrophys. J. Lett.* **875** (2019) L1 [1906.11238].
- [8] **Event Horizon Telescope** Collaboration, K. Akiyama *et al.*, *First M87 Event Horizon Telescope Results. II. Array and Instrumentation*, *Astrophys. J. Lett.* **875** (2019), no. 1, L2 [1906.11239].
- [9] **Event Horizon Telescope** Collaboration, K. Akiyama *et al.*, *First M87 Event Horizon Telescope Results. III. Data Processing and Calibration*, *Astrophys. J. Lett.* **875** (2019), no. 1, L3 [1906.11240].
- [10] **Event Horizon Telescope** Collaboration, K. Akiyama *et al.*, *First M87 Event Horizon Telescope Results. IV. Imaging the Central Supermassive Black Hole*, *Astrophys. J. Lett.* **875** (2019), no. 1, L4 [1906.11241].
- [11] **Event Horizon Telescope** Collaboration, K. Akiyama *et al.*, *First M87 Event Horizon Telescope Results. V. Physical Origin of the Asymmetric Ring*, *Astrophys. J. Lett.* **875** (2019), no. 1, L5 [1906.11242].
- [12] **Event Horizon Telescope** Collaboration, K. Akiyama *et al.*, *First M87 Event Horizon Telescope Results. VI. The Shadow and Mass of the Central Black Hole*, *Astrophys. J. Lett.* **875** (2019), no. 1, L6 [1906.11243].
- [13] **Event Horizon Telescope** Collaboration, K. Akiyama *et al.*, *First Sagittarius A* Event Horizon Telescope Results. I. The Shadow of the Supermassive Black Hole in the Center of the Milky Way*, *Astrophys. J. Lett.* **930** (2022), no. 2, L12.
- [14] **Event Horizon Telescope** Collaboration, K. Akiyama *et al.*, *First Sagittarius A* Event Horizon Telescope Results. II. EHT and Multiwavelength Observations, Data Processing, and Calibration*, *Astrophys. J. Lett.* **930** (2022), no. 2, L13.
- [15] **Event Horizon Telescope** Collaboration, K. Akiyama *et al.*, *First Sagittarius A* Event Horizon Telescope Results. III. Imaging of the Galactic Center Supermassive Black Hole*, *Astrophys. J. Lett.* **930** (2022), no. 2, L14.

- [16] **Event Horizon Telescope** Collaboration, K. Akiyama *et al.*, *First Sagittarius A* Event Horizon Telescope Results. IV. Variability, Morphology, and Black Hole Mass*, *Astrophys. J. Lett.* **930** (2022), no. 2, L15.
- [17] **Event Horizon Telescope** Collaboration, K. Akiyama *et al.*, *First Sagittarius A* Event Horizon Telescope Results. V. Testing Astrophysical Models of the Galactic Center Black Hole*, *Astrophys. J. Lett.* **930** (2022), no. 2, L16.
- [18] **Event Horizon Telescope** Collaboration, K. Akiyama *et al.*, *First Sagittarius A* Event Horizon Telescope Results. VI. Testing the Black Hole Metric*, *Astrophys. J. Lett.* **930** (2022), no. 2, L17.
- [19] **Event Horizon Telescope** Collaboration, P. Kocherlakota *et al.*, *Constraints on black-hole charges with the 2017 EHT observations of M87**, *Phys. Rev. D* **103** (2021), no. 10, 104047 [2105.09343].
- [20] **LIGO Scientific, Virgo** Collaboration, B. P. Abbott *et al.*, *Tests of General Relativity with the Binary Black Hole Signals from the LIGO-Virgo Catalog GWTC-1*, *Phys. Rev. D* **100** (2019), no. 10, 104036 [1903.04467].
- [21] **LIGO Scientific, VIRGO, KAGRA** Collaboration, R. Abbott *et al.*, *Tests of General Relativity with GWTC-3*, 2112.06861.
- [22] D. Psaltis, *Testing General Relativity with the Event Horizon Telescope*, *Gen. Rel. Grav.* **51** (2019), no. 10, 137 [1806.09740].
- [23] E. Himwich, M. D. Johnson, A. Lupasca and A. Strominger, *Universal polarimetric signatures of the black hole photon ring*, *Phys. Rev. D* **101** (2020), no. 8, 084020 [2001.08750].
- [24] S. E. Gralla, *Can the EHT M87 results be used to test general relativity?*, *Phys. Rev. D* **103** (2021), no. 2, 024023 [2010.08557].
- [25] S. Vagnozzi, R. Roy, Y.-D. Tsai and L. Visinelli, *Horizon-scale tests of gravity theories and fundamental physics from the Event Horizon Telescope image of Sagittarius A**, 2205.07787.
- [26] S. H. Völkel, E. Barausse, N. Franchini and A. E. Broderick, *EHT tests of the strong-field regime of general relativity*, *Class. Quant. Grav.* **38** (2021), no. 21, 21LT01 [2011.06812].

- [27] C. Bambi, K. Freese, S. Vagnozzi and L. Visinelli, *Testing the rotational nature of the supermassive object M87* from the circularity and size of its first image*, Phys. Rev. D **100** (2019), no. 4, 044057 [1904.12983].
- [28] S. Vagnozzi and L. Visinelli, *Hunting for extra dimensions in the shadow of M87**, Phys. Rev. D **100** (2019), no. 2, 024020 [1905.12421].
- [29] A. Allahyari, M. Khodadi, S. Vagnozzi and D. F. Mota, *Magnetically charged black holes from non-linear electrodynamics and the Event Horizon Telescope*, JCAP **02** (2020) 003 [1912.08231].
- [30] M. Khodadi, A. Allahyari, S. Vagnozzi and D. F. Mota, *Black holes with scalar hair in light of the Event Horizon Telescope*, JCAP **09** (2020) 026 [2005.05992].
- [31] K. S. Virbhadra and G. F. R. Ellis, *Schwarzschild black hole lensing*, Phys. Rev. D **62** (2000) 084003 [astro-ph/9904193].
- [32] A. Bhadra, *Gravitational lensing by a charged black hole of string theory*, Phys. Rev. D **67** (2003) 103009 [gr-qc/0306016].
- [33] S. Chen and J. Jing, *Strong field gravitational lensing in the deformed Hořava-Lifshitz black hole*, Phys. Rev. D **80** (Jul, 2009) 024036.
- [34] E. F. Eiroa, *Gravitational lensing by Einstein-Born-Infeld black holes*, Phys. Rev. D **73** (2006) 043002 [gr-qc/0511065].
- [35] M. Bartelmann and M. Maturi, *Weak gravitational lensing*, Scholarpedia **12** (2017), no. 1, 32440 [1612.06535].
- [36] T. G. Brainerd, R. D. Blandford and I. Smail, *Measuring galaxy masses using galaxy - galaxy gravitational lensing*, Astrophys. J. **466** (1996) 623 [astro-ph/9503073].
- [37] S. Frittelli, T. P. Kling and E. T. Newman, *Space-time perspective of Schwarzschild lensing*, Phys. Rev. D **61** (2000) 064021 [gr-qc/0001037].
- [38] V. Bozza, *Gravitational lensing in the strong field limit*, Phys. Rev. D **66** (2002) 103001 [gr-qc/0208075].
- [39] A. B. Congdon and C. R. Keeton, *Principles of Gravitational Lensing*. Springer Praxis Books. Springer Cham, Springer International Publishing AG, 2018.

- [40] V. Bozza, *Quasiequatorial gravitational lensing by spinning black holes in the strong field limit*, Phys. Rev. D **67** (2003) 103006 [gr-qc/0210109].
- [41] V. Bozza, *A Comparison of approximate gravitational lens equations and a proposal for an improved new one*, Phys. Rev. D **78** (2008) 103005 [0807.3872].
- [42] A. Einstein, *Lens-Like Action of a Star by the Deviation of Light in the Gravitational Field*, Science **84** (1936) 506–507.
- [43] E. F. Eiroa and C. M. Sendra, *Gravitational lensing by a regular black hole*, Class. Quant. Grav. **28** (2011) 085008 [1011.2455].
- [44] A. Y. Bin-Nun, *Strong Gravitational Lensing by Sgr A**, Class. Quant. Grav. **28** (2011) 114003 [1011.5848].
- [45] L. Amarilla, E. F. Eiroa and G. Giribet, *Null geodesics and shadow of a rotating black hole in extended Chern-Simons modified gravity*, Phys. Rev. D **81** (2010) 124045 [1005.0607].
- [46] I. Z. Stefanov, S. S. Yazadjiev and G. G. Gyulchev, *Connection between Black-Hole Quasinormal Modes and Lensing in the Strong Deflection Limit*, Phys. Rev. Lett. **104** (2010) 251103 [1003.1609].
- [47] S.-W. Wei, Y.-X. Liu, C.-E. Fu and K. Yang, *Strong field limit analysis of gravitational lensing in Kerr-Taub-NUT spacetime*, JCAP **10** (2012) 053 [1104.0776].
- [48] S. Chen, Y. Liu and J. Jing, *Strong gravitational lensing in a squashed Kaluza-Klein Gödel black hole*, Phys. Rev. D **83** (2011) 124019 [1102.0086].
- [49] G. N. Gyulchev and I. Z. Stefanov, *Gravitational Lensing by Phantom Black holes*, Phys. Rev. D **87** (2013), no. 6, 063005 [1211.3458].
- [50] N. Tsukamoto, T. Harada and K. Yajima, *Can we distinguish between black holes and wormholes by their Einstein ring systems?*, Phys. Rev. D **86** (2012) 104062 [1207.0047].
- [51] S. Sahu, M. Patil, D. Narasimha and P. S. Joshi, *Can strong gravitational lensing distinguish naked singularities from black holes?*, Phys. Rev. D **86** (2012) 063010 [1206.3077].

- [52] S. Chen and J. Jing, *Strong gravitational lensing by a rotating non-Kerr compact object*, Phys. Rev. D **85** (2012) 124029 [1204.2468].
- [53] S.-W. Wei and Y.-X. Liu, *Observing the shadow of Einstein-Maxwell-Dilaton-Axion black hole*, JCAP **11** (2013) 063 [1311.4251].
- [54] F. Atamurotov, A. Abdujabbarov and B. Ahmedov, *Shadow of rotating non-Kerr black hole*, Phys. Rev. D **88** (2013), no. 6, 064004.
- [55] E. F. Eiroa and C. M. Sendra, *Regular phantom black hole gravitational lensing*, Phys. Rev. D **88** (2013), no. 10, 103007 [1308.5959].
- [56] S.-W. Wei, K. Yang and Y.-X. Liu, *Black hole solution and strong gravitational lensing in Eddington-inspired Born-Infeld gravity*, Eur. Phys. J. C **75** (2015) 253 [1405.2178], [Erratum: Eur.Phys.J.C 75, 331 (2015)].
- [57] N. Tsukamoto, T. Kitamura, K. Nakajima and H. Asada, *Gravitational lensing in Tangherlini spacetime in the weak gravitational field and the strong gravitational field*, Phys. Rev. D **90** (2014), no. 6, 064043 [1402.6823].
- [58] X. Liu, J. Jia and N. Yang, *Gravitational lensing of massive particles in Schwarzschild gravity*, Class. Quant. Grav. **33** (2016), no. 17, 175014 [1512.04037].
- [59] S. W. Wei, Y. X. Liu and C. E. Fu, *Null Geodesics and Gravitational Lensing in a Nonsingular Spacetime*, Adv. High Energy Phys. **2015** (2015) 454217 [1510.02560].
- [60] H. Sotani and U. Miyamoto, *Strong gravitational lensing by an electrically charged black hole in Eddington-inspired Born-Infeld gravity*, Phys. Rev. D **92** (2015), no. 4, 044052 [1508.03119].
- [61] G. S. Bisnovatyi-Kogan and O. Y. Tsupko, *Gravitational Lensing in Plasmic Medium*, Plasma Phys. Rep. **41** (2015) 562 [1507.08545].
- [62] M. Sharif and S. Iftikhar, *Strong gravitational lensing in non-commutative wormholes*, Astrophys. Space Sci. **357** (2015), no. 1, 85.
- [63] A. Younas, S. Hussain, M. Jamil and S. Bahamonde, *Strong Gravitational Lensing by Kiselev Black Hole*, Phys. Rev. D **92** (2015), no. 8, 084042 [1502.01676].

- [64] S. Chen and J. Jing, *Strong gravitational lensing for the photons coupled to Weyl tensor in a Schwarzschild black hole spacetime*, JCAP **10** (2015) 002 [1502.01088].
- [65] J. Schee, Z. Stuchlík, B. Ahmedov, A. Abdujabbarov and B. Toshmatov, *Gravitational lensing by regular black holes surrounded by plasma*, Int. J. Mod. Phys. D **26** (2017), no. 5, 1741011.
- [66] J. Man and H. Cheng, *Analytical discussion on strong gravitational lensing for a massive source with a $f(R)$ global monopole*, Phys. Rev. D **92** (2015), no. 2, 024004 [1205.4857].
- [67] N. Tsukamoto, *Deflection angle in the strong deflection limit in a general asymptotically flat, static, spherically symmetric spacetime*, Phys. Rev. D **95** (2017), no. 6, 064035 [1612.08251].
- [68] S. Wang, S. Chen and J. Jing, *Strong gravitational lensing by a Konoplya-Zhidenko rotating non-Kerr compact object*, JCAP **11** (2016) 020 [1609.00802].
- [69] N. Tsukamoto, *Strong deflection limit analysis and gravitational lensing of an Ellis wormhole*, Phys. Rev. D **94** (2016), no. 12, 124001 [1607.07022].
- [70] F. Zhao, J. Tang and F. He, *Gravitational lensing effects of a Reissner–Nordstrom–de Sitter black hole*, Phys. Rev. D **93** (2016), no. 12, 123017.
- [71] G. F. Aldi and V. Bozza, *Relativistic iron lines in accretion disks: the contribution of higher order images in the strong deflection limit*, JCAP **02** (2017) 033 [1607.05365].
- [72] X. Lu, F.-W. Yang and Y. Xie, *Strong gravitational field time delay for photons coupled to Weyl tensor in a Schwarzschild black hole*, Eur. Phys. J. C **76** (2016), no. 7, 357 [1606.02932].
- [73] R. T. Cavalcanti, A. G. da Silva and R. da Rocha, *Strong deflection limit lensing effects in the minimal geometric deformation and Casadio–Fabbri–Mazzacurati solutions*, Class. Quant. Grav. **33** (2016), no. 21, 215007 [1605.01271].
- [74] S.-S. Zhao and Y. Xie, *Strong field gravitational lensing by a charged Galileon black hole*, JCAP **07** (2016) 007 [1603.00637].
- [75] R. Shaikh and S. Kar, *Gravitational lensing by scalar-tensor wormholes and the energy conditions*, Phys. Rev. D **96** (2017), no. 4, 044037 [1705.11008].

- [76] M. Rahman and A. A. Sen, *Astrophysical Signatures of Black holes in Generalized Proca Theories*, Phys. Rev. D **99** (2019), no. 2, 024052 [1810.09200].
- [77] K. S. Virbhadra, *Distortions of images of Schwarzschild lensing*, 2204.01879.
- [78] T. Hsieh, D.-S. Lee and C.-Y. Lin, *Strong gravitational lensing by Kerr and Kerr-Newman black holes*, Phys. Rev. D **103** (2021), no. 10, 104063 [2101.09008].
- [79] T. Hsieh, D.-S. Lee and C.-Y. Lin, *Gravitational time delay effects by Kerr and Kerr-Newman black holes in strong field limits*, Phys. Rev. D **104** (2021), no. 10, 104013 [2108.05006].
- [80] A. Edery and J. Godin, *Second order Kerr deflection*, Gen. Rel. Grav. **38** (2006) 1715–1722.
- [81] V. Perlick and O. Y. Tsupko, *Calculating black hole shadows: Review of analytical studies*, Phys. Rept. **947** (2022) 1–39 [2105.07101].
- [82] P. V. P. Cunha, C. A. R. Herdeiro, E. Radu and H. F. Runarsson, *Shadows of Kerr black holes with scalar hair*, Phys. Rev. Lett. **115** (2015), no. 21, 211102 [1509.00021].
- [83] M. Wang, S. Chen and J. Jing, *Shadow casted by a Konoplya-Zhidenko rotating non-Kerr black hole*, JCAP **10** (2017) 051 [1707.09451].
- [84] Z. Younsi, A. Zhidenko, L. Rezzolla, R. Konoplya and Y. Mizuno, *New method for shadow calculations: Application to parametrized axisymmetric black holes*, Phys. Rev. D **94** (2016), no. 8, 084025 [1607.05767].
- [85] G. S. Bisnovatyi-Kogan and O. Y. Tsupko, *Shadow of a black hole at cosmological distances*, Phys. Rev. D **98** (2018), no. 8, 084020 [1805.03311].
- [86] I. Banerjee, S. Chakraborty and S. SenGupta, *Silhouette of M87*: A New Window to Peek into the World of Hidden Dimensions*, Phys. Rev. D **101** (2020), no. 4, 041301 [1909.09385].
- [87] O. Y. Tsupko and G. S. Bisnovatyi-Kogan, *First analytical calculation of black hole shadow in McVittie metric*, Int. J. Mod. Phys. D **29** (2020), no. 09, 2050062 [1912.07495].

- [88] O. Y. Tsupko, Z. Fan and G. S. Bisnovatyi-Kogan, *Black hole shadow as a standard ruler in cosmology*, *Class. Quant. Grav.* **37** (2020), no. 6, 065016 [1905.10509].
- [89] A. K. Mishra, S. Chakraborty and S. Sarkar, *Understanding photon sphere and black hole shadow in dynamically evolving spacetimes*, *Phys. Rev. D* **99** (2019), no. 10, 104080 [1903.06376].
- [90] S. Vagnozzi, C. Bambi and L. Visinelli, *Concerns regarding the use of black hole shadows as standard rulers*, *Class. Quant. Grav.* **37** (2020), no. 8, 087001 [2001.02986].
- [91] P.-C. Li, M. Guo and B. Chen, *Shadow of a Spinning Black Hole in an Expanding Universe*, *Phys. Rev. D* **101** (2020), no. 8, 084041 [2001.04231].
- [92] V. Perlick and O. Y. Tsupko, *Light propagation in a plasma on Kerr spacetime: Separation of the Hamilton-Jacobi equation and calculation of the shadow*, *Phys. Rev. D* **95** (2017), no. 10, 104003 [1702.08768].
- [93] S.-W. Wei, Y.-X. Liu and R. B. Mann, *Intrinsic curvature and topology of shadows in Kerr spacetime*, *Phys. Rev. D* **99** (2019), no. 4, 041303 [1811.00047].
- [94] A. Chowdhuri and A. Bhattacharyya, *Shadow analysis for rotating black holes in the presence of plasma for an expanding universe*, *Phys. Rev. D* **104** (2021), no. 6, 064039 [2012.12914].
- [95] U. Papnoi, F. Atamurotov, S. G. Ghosh and B. Ahmedov, *Shadow of five-dimensional rotating Myers-Perry black hole*, *Phys. Rev. D* **90** (2014), no. 2, 024073 [1407.0834].
- [96] L. Amarilla and E. F. Eiroa, *Shadow of a Kaluza-Klein rotating dilaton black hole*, *Phys. Rev. D* **87** (2013), no. 4, 044057 [1301.0532].
- [97] L. Amarilla and E. F. Eiroa, *Shadow of a rotating braneworld black hole*, *Phys. Rev. D* **85** (2012) 064019 [1112.6349].
- [98] S. Sarkar, S. Kumar and S. Bhattacharjee, *Can we detect a supertranslated black hole?*, *Phys. Rev. D* **105** (2022), no. 8, 084001 [2110.03547].
- [99] F.-L. Lin, A. Patel and H.-Y. Pu, *Black Hole Shadow with Soft Hair*, 2202.13559.

- [100] S. Chandrasekhar, *The mathematical theory of black holes*. Oxford classic texts in the physical sciences. Oxford Univ. Press, Oxford, 2002.
- [101] S. L. Adler and K. S. Virbhadra, *Cosmological constant corrections to the photon sphere and black hole shadow radii*, 2205.04628.
- [102] K. S. Virbhadra, *Compactness of supermassive dark objects at galactic centers*, 2204.01792.
- [103] R. Roy, S. Vagnozzi and L. Visinelli, *Superradiance evolution of black hole shadows revisited*, Phys. Rev. D **105** (2022), no. 8, 083002 [2112.06932].
- [104] Y. Chen, R. Roy, S. Vagnozzi and L. Visinelli, *Superradiant evolution of the shadow and photon ring of Sgr A**, 2205.06238.
- [105] A. Simpson and M. Visser, *Black-bounce to traversable wormhole*, JCAP **02** (2019) 042 [1812.07114].
- [106] F. S. N. Lobo, M. E. Rodrigues, M. V. d. S. Silva, A. Simpson and M. Visser, *Novel black-bounce spacetimes: wormholes, regularity, energy conditions, and causal structure*, Phys. Rev. D **103** (2021), no. 8, 084052 [2009.12057].
- [107] J. Mazza, E. Franzin and S. Liberati, *A novel family of rotating black hole mimickers*, JCAP **04** (2021) 082 [2102.01105].
- [108] E. Franzin, S. Liberati, J. Mazza, A. Simpson and M. Visser, *Charged black-bounce spacetimes*, JCAP **07** (2021) 036 [2104.11376].
- [109] N. Tsukamoto, *Gravitational lensing in the Simpson-Visser black-bounce spacetime in a strong deflection limit*, Phys. Rev. D **103** (2021), no. 2, 024033 [2011.03932].
- [110] J. R. Nascimento, A. Y. Petrov, P. J. Porfirio and A. R. Soares, *Gravitational lensing in black-bounce spacetimes*, Phys. Rev. D **102** (2020), no. 4, 044021 [2005.13096].
- [111] M. Guerrero, G. J. Olmo, D. Rubiera-Garcia and D. S.-C. Gómez, *Shadows and optical appearance of black bounces illuminated by a thin accretion disk*, JCAP **08** (2021) 036 [2105.15073].
- [112] S. U. Islam, J. Kumar and S. G. Ghosh, *Strong gravitational lensing by rotating Simpson-Visser black holes*, JCAP **10** (2021) 013 [2104.00696].

- [113] Y. Guo and Y.-G. Miao, *Charged black-bounce spacetimes: Photon rings, shadows and observational appearances*, 2112.01747.
- [114] J. Zhang and Y. Xie, *Gravitational lensing by a black-bounce-Reissner–Nordström spacetime*, Eur. Phys. J. C **82** (2022), no. 5, 471.
- [115] S. V. Iyer and E. C. Hansen, *Light’s Bending Angle in the Equatorial Plane of a Kerr Black Hole*, Phys. Rev. D **80** (2009) 124023 [0907.5352].
- [116] Y.-W. Hsiao, D.-S. Lee and C.-Y. Lin, *Equatorial light bending around Kerr-Newman black holes*, Phys. Rev. D **101** (2020), no. 6, 064070 [1910.04372].
- [117] C.-M. Claudel, K. S. Virbhadra and G. F. R. Ellis, *The Geometry of photon surfaces*, J. Math. Phys. **42** (2001) 818–838 [gr-qc/0005050].
- [118] T. Müller, *Einstein rings as a tool for estimating distances and the mass of a Schwarzschild black hole*, Phys. Rev. D **77** (Jun, 2008) 124042.
- [119] K. S. Virbhadra, *Relativistic images of Schwarzschild black hole lensing*, Phys. Rev. D **79** (2009) 083004 [0810.2109].
- [120] V. Bozza, S. Capozziello, G. Iovane and G. Scarpetta, *Strong field limit of black hole gravitational lensing*, Gen. Rel. Grav. **33** (2001) 1535–1548 [gr-qc/0102068].
- [121] S.-W. Wei, Y.-C. Zou, Y.-X. Liu and R. B. Mann, *Curvature radius and Kerr black hole shadow*, JCAP **08** (2019) 030 [1904.07710].
- [122] K. Hioki and K.-i. Maeda, *Measurement of the Kerr Spin Parameter by Observation of a Compact Object’s Shadow*, Phys. Rev. D **80** (2009) 024042 [0904.3575].
- [123] S. E. Gralla, D. E. Holz and R. M. Wald, *Black Hole Shadows, Photon Rings, and Lensing Rings*, Phys. Rev. D **100** (2019), no. 2, 024018 [1906.00873].
- [124] S. Kasuya and M. Kobayashi, *Throat effects on shadows of Kerr-like wormholes*, Phys. Rev. D **103** (2021), no. 10, 104050 [2103.13086].
- [125] J. Barrientos, A. Cisterna, N. Mora and A. Viganò, *AdS-Taub-NUT spacetimes and exact black bounces with scalar hair*, Phys. Rev. D **106** (2022), no. 2, 024038 [2202.06706].

- [126] Y. Hou, P. Liu, M. Guo, H. Yan and B. Chen, *Multi-level images around Kerr-Newman black holes*, 2203.02755.
- [127] G. S. Bisnovatyi-Kogan and O. Y. Tsupko, *Gravitational Lensing in Presence of Plasma: Strong Lens Systems, Black Hole Lensing and Shadow*, Universe **3** (2017), no. 3, 57 [1905.06615].
- [128] S. Hadar, M. D. Johnson, A. Lupsasca and G. N. Wong, *Photon Ring Autocorrelations*, Phys. Rev. D **103** (2021), no. 10, 104038 [2010.03683].